Remodeling of Murine Vaginal Smooth Muscle Function with Reproductive Age and Elastic Fiber Disruption

Shelby E. White*[1], Niyousha Karbasion*[2], J. Caleb Snider, Ph.D.[2], Maria Florian-Rodriguez, M.D.[3], Matthew R. Bersi[2], Ph.D., Kristin S. Miller, Ph.D**.[3,4,5]**

***,** Denotes equal contributions to the work**

1. **Department of Biomedical Engineering, Tulane University, New Orleans, LA, USA.**
2. **Department of Mechanical Engineering & Materials Science, Washington University in St. Louis, St. Louis, MO, USA.**
3. **Department of Obstetrics and Gynecology, University of Texas Southwestern Medical Center, Dallas, TX, USA**
4. **Department of Mechanical Engineering, University of Texas at Dallas, Richardson, TX, USA**
5. **Department of Bioengineering, University of Texas at Dallas, Richardson, TX, USA**

Abstract

Advanced maternal age during pregnancy is associated with increased risk of vaginal tearing during delivery and maladaptive postpartum healing. Although the underlying mechanisms of age-related vaginal injuries are not fully elucidated, changes in vaginal microstructure may contribute. Smooth muscle cells promote the contractile nature of the vagina and contribute to pelvic floor stability. While menopause is associated with decreased vaginal smooth muscle content, whether contractile changes occur before the onset of menopause remains unknown. Therefore, the first objective of this study was to quantify the active mechanical behavior of the murine vagina with age. Further, aging is associated with decreased vaginal elastin content. As such, the second objective was to determine if elastic fiber disruption alters vaginal contractility. Vaginal samples from mice aged 2-14 months were used in maximum contractility experiments and biaxial extension-inflation protocols. To evaluate the role of elastic fibers with age, half of the vaginal samples were randomly allocated to enzymatic elastic fiber disruption. Contractile potential decreased and vaginal material stiffness increased with age. These age-related changes in smooth muscle function may be due, in part, to changes in microstructural composition or contractile gene expression. Furthermore, elastic fiber disruption had a diminished effect on smooth muscle contractility in older mice. This suggests a decreased functional role of elastic fibers with age. Quantifying the age-dependent mechanical contribution of smooth muscle cells and elastic fibers to vaginal properties provides a first step towards better understanding how age-related changes in vaginal structure may contribute to tissue integrity and healing.

Graphical abstract :

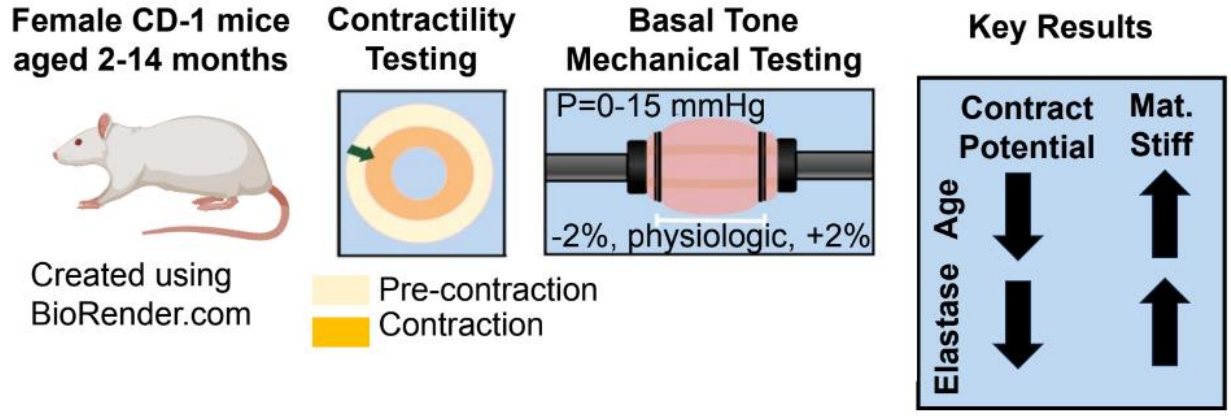

1. Introduction

The vagina is a soft, muscular, organ that continuously adapts to biomechanical and biochemical signals in order to facilitate physiologic processes, such as pelvic floor function, sexual activity, passage for menstrual blood and tissue, and childbirth [1]. Maternal age at the time of pregnancy has long been associated with increased rates of obstetric complications [2]; however, the link between age and vaginal wall properties remains unknown. A better understanding of the mechanobiological factors that increase the risk of age-related childbirth complications is needed, given that 9x more people are delaying childbirth today compared to forty years ago [3]. This increase in maternal age is associated with higher risk of gestational diabetes, preeclampsia, and severe vaginal tearing during childbirth [4-6] as well as pathologies such as sexual dysfunction and vaginal atrophy [7, 8]. While the etiology of increased age-related risk for obstetric trauma or pathology development is not well-defined, remodeling of the cellular and extracellular matrix (ECM) composition of the vagina may contribute to adverse outcomes [9].

Among the primary cellular constituents in the vaginal wall, smooth muscle cells contribute to the contractile nature of the tissue. Vaginal contractility facilitates biological functions such as menstruation, intercourse, and childbirth. In addition to active contractility, smooth muscle cells contribute to maintaining pelvic floor support through their attachment to structural supports (e.g., levator ani) and baseline contraction [10]. This baseline contractile level in the absence of external stimuli is known as basal tone [11, 12]. Studies investigating the changes in mechanical properties of the vagina with age are limited and largely focused on changes following menopause and the onset of pelvic organ prolapse in humans [13-15]. However, it is generally observed in other contractile soft tissues, such as the systemic vasculature, that smooth muscle content and the expression of genes encoding contractile proteins such as alpha- smooth muscle actin (gene: *Acta2*) and myosin heavy chain (gene: *Myh11*) decrease with age [16]. Thus, there is a need to investigate age-dependent changes in vaginal contractile properties.

The vagina is a tissue that is subjected to multiaxial loads in the body while undergoing everyday activities such as standing, walking, lifting over 10 pounds, and coughing [17-19]. [17-19]. This directional behavior may be due to direction-specific orientations of cellular and extracellular matrix components, such as smooth muscle cells, elastic fibers, and collagen fibers [20-22]. The use of biaxial extension-inflation protocols permits quantification of the circumferential and longitudinal passive and active mechanical properties, while maintaining native smooth muscle cell- extracellular matrix interactions and organ geometry [23]. Previously, we investigated the passive biaxial response of the murine vagina aged from 2-14 months. Therein, we observed age-related stiffening and decreased mechanical contributions of elastic fibers to the passive mechanical properties of the vagina [24].

Elastic fibers provide the compliant nature of the vagina and allow for the organ to stretch and recoil in response to changes in intra-abdominal pressures [25, 26]. Further, elastic fibers maintain the geometry of the vagina and may constrain collagen undulation thereby contributing further to vaginal resistance to deformation [9, 27]. In most organs, elastic fiber production occurs during gestational development with negligent synthesis in adult

tissues. In the female reproductive system, however, it is suggested that there may be a potential burst of elastic fiber synthesis and cross-linking occurs in the vaginal wall postpartum [70, 71]. Moreover, decreased elastic fiber content and subsequent loss of tissue elasticity is associated with aging, however, the rate at which elastic fibers may be disrupted with age is not well understood [28, 29]. Previously, enzymatic disruption of elastic fibers via elastase treatment resulted in an increased outer diameter, decreased compliance, and increased circumferential stress of the C57BL/6 mouse aged 4-6 months [30]. Moreover, the longitudinal distribution of elastic fibers in the C57BL/6 murine vagina exhibited a greater area fraction compared to the circumferential orientation [30]. While we have previously characterized the passive mechanical behavior following elastic fiber degradation with age [24], the composition of elastic fibers, and consequently, their biaxial mechanical contribution in the active (contractile) state remains unknown.

Further, there may be changes in vaginal contractility following elastic fiber disruption with age, as vaginal contractility decreased in the longitudinal direction in a nulliparous (nonpregnant) murine model following enzymatic elastic fiber disruption [22]. Additionally, age-related changes in the content and organization of the cellular and microstructural components within the vaginal wall are not well characterized [31, 32]. Given the lack of compositional information, it is likely that the overall contractile function of the vagina is dependent on the microstructural arrangement and its impact on vaginal smooth muscle mechanobiology. Therefore, there is a need to investigate both the contractile function (at multiple length scales) and microstructural composition of the vagina.

Animal models, such as mice, may offer potential benefits to studying vaginal wall remodeling as an alternative to human vaginal tissue samples, which have limited availability and significant biological variation across patients. Because the fetal head is smaller than that of humans relative to the vaginal canal, mice do not naturally sustain injuries during birth [33]. Despite relative anatomical differences, rodents are widely used to investigate the pelvic floor in various healthy or diseased states due to the benefits of a predictive estrous cycle and well-documented age correlations to the human throughout menopause [34]. Additionally, both the human and murine vagina are considered to be fibromuscular organs with a well-defined layered structure comprised of load bearing collagen and elastic fibers and contractile smooth muscle cells. Hence, mouse models may be leveraged to provide key insights into the microstructural remodeling and altered mechanical function of the vagina that contribute to aging and its associated pathologies [35, 36].

Therefore, the primary objectives of the study were to (i) quantify the circumferential and longitudinal contractile potential and biomechanical function of the murine vagina and (ii) assess age-induced changes in the vaginal microstructural organization in the nonpregnant murine vagina. Here, we hypothesized smooth muscle function would show direction-dependent behavior, decrease with age, and coincide with decreased smooth muscle content and altered elastic fiber organization. Additionally, the secondary objectives of the study were to evaluate the functional contribution of elastic fibers to the active mechanical properties of the vagina by (i) measuring vaginal contractility and basal tone in age-matched control and elastase treated samples and (ii) determining the

associated alterations in microstructural composition and gene expression profiles of the vaginal wall. Here, we hypothesized that in the active state, elastic fiber disruption via elastase treatment would be associated with decreased vaginal contractility and increased material stiffness in the circumferential and longitudinal directions. Further, we hypothesized the mechanical contribution of elastic fibers to active mechanical properties of the vagina would decrease with age.

2. Methods

2.1 Pressure Catheterization.

Pressure catheter measurements were taken longitudinally in female nulliparous CD-1 mice at estrus starting at 2 months of age and repeated every three weeks until the mice were 14 months old. Pressure catheter experiments were performed as described previously [22, 24]. Briefly, a 3 mm balloon was fabricated with polyvinyl chloride and secured with 6-0 silk sutures around a 1.25 mm aluminum tube. Mice were anesthetized with 3% isoflurane in 100% oxygen, and 1.5 mL of water was pushed into the balloon to obtain ambient air pressure. The inflated balloon was then inserted through the vaginal opening (introitus) into the vaginal canal. Vaginal pressure was measured as the change between ambient conditions and the pressure once inflated inside the vaginal canal [17]. For each experiment, the process was repeated a total of 3 times on each animal and averaged for one data point. Longitudinal pressure measurements (n=9/ age group) were averaged for different mice at 2-3 months, 4-6 months, 7-9 months, and 10-14 months of age.

2.2 Animals.

A total of n=64 (16/ age group) nulliparous female CD-1 mice were housed in a 12-hour light/ dark cycle room and provided a standard chow diet and access to water ad libitum. The vagina was visually determined to be at estrus by lifting the tail and examining the vaginal opening width and surrounding tissues' redness [37]. Before dissection, mice were weighed on a digital scale. To preserve smooth muscle cell viability, mice were euthanized at estrus via guillotine without anesthesia (Tulane IACUC approved).

2.3 Sample Preparation and Cannulation.

Upon sacrifice, the reproductive system was dissected and immediately placed in cold (4 °C) Hank's Balanced Salt Solution (HBSS). The vaginal canal was separated from the upper reproductive organs by a singular cut between the cervix and vagina. Following dissection, the vagina was secured onto cannulas in a custom-built biaxial extension-inflation pressure myograph (Danish MyoTechnologies, Aarhus, Denmark). Two silk 6-0 sutures were tied to each end of the vagina and secured with forceps. The proximal end of the vagina was cannulated onto the fluid inlet and the distal end of the vagina to the fluid outlet of the pressure myograph.

2.4 Biomechanical Phenotyping and Contractile Potential.

Established extension-inflation protocols assessed the biaxial mechanical properties of the vagina while maintaining the native cell-matrix interactions and tubular geometry of the vagina [38-41]. Briefly, the vagina was stretched to the measured in-situ physiologic

length prior to extraction from the body and was pressurized to the unloaded pressure. The unloaded pressure was identified as the first pressure at which the vagina is no longer collapsed [22, 30, 38]. The longitudinal length was then decreased at a rate of 10 μm/s until there was a minimal change in longitudinal force, which was defined as the unloaded length.

To minimize hysteresis and ensure consistent and repeatable measurements, the vagina was preconditioned from 0 mmHg to the mean in vivo pressure for five cycles at a rate of 1.5 mmHg/s [30, 42]. For circumferential preconditioning, the vagina underwent five pressurization cycles (0-15 mmHg) at the physiologic length whereas longitudinal preconditioning was performed at longitudinal extensions from -2% to +2% of the physiologic length at 1/3 of the maximum pressure [40, 41, 43]. To precondition the vaginal smooth muscle cell contractile response, the bath was heated to 37 °C and the vagina was set to the physiologic length and pressurized to the mean in vivo pressure. The vagina was then stimulated with 40 mM potassium chloride (KCl) for 5 minutes until a steady contractile response was achieved [44]. Post-stimulation, the bath was washed twice with Krebs Ringer Buffer Solution (KRBs) to return the longitudinal force to basal tone. The tissue was then equilibrated for 10 minutes at the physiologic length and basal tone, followed by re-establishment of the unloaded configuration [38, 45].

To assess the maximum contractile potential of the vagina, the tissue was set at the physiologic length and physiologic pressure and stimulated with 40 mM KCl for 5 minutes [22]. To assess the contribution of basal tone to vaginal biomechanics, tissues were then subjected to five cycles of pressure-diameter testing from 0-15 mmHg at the physiologic length and $\pm$2% of the physiologic length. To confirm the physiologic length based on an energetically-preferred longitudinal force-stretch cross-over point [46], the vagina was longitudinally extended from -2% to +2% of the physiologic length under four constant pressures: tare load (2 mmHg), one-third maximum pressure (5 mmHg), two-thirds maximum pressure (10 mmHg), and the maximum pressure (15 mmHg) [22, 30, 38].

2.5 Elastic Fiber Disruption via Elastase Treatment.

Prior to mechanical testing, an automated number generator randomly allocated vaginal samples to either elastase treatment or untreated control groups. For elastase treatment to induce elastic fiber degradation, the vagina was intraluminally treated with 15 U porcine pancreatic elastase (ThermoFisher, J61874MC) for 45 minutes [9, 30]. The elastase concentration and incubation time were selected from additional studies in C57BL/6 mice wherein histological analysis demonstrated significantly less elastin area fraction after treatment [30]. For samples randomly allocated to the elastase treatment group, contractility protocols and basal tone pressure-diameter and force-length tests were repeated after elastase treatment.

2.6 Biomechanical Data Analysis.

To assess the maximum contractile potential of the vagina, the longitudinal contractile potential was defined as the change in longitudinal force between the initial longitudinal force prior to stimulation ($F_{initial}$) and peak force achieved during contraction (F_{cont}; equation 1) [22]. The circumferential contractile potential was calculated by the change in

outer diameter between the initial outer diameter prior to stimulation ($OD_{initial}$) and the outer diameter after exposure to the vasoactive stimulation (OD_{cont}) via KCl treatment (equation 2).

$$Longitudinal\ Contractile\ Potential = \Delta\ Longitudinal\ Force \quad \text{(Equation 1)}$$

$$Circumferential\ Contractile\ Potential = \Delta\ Outer\ Diameter \quad \text{(Equation 2)}$$

The vaginal canal geometry was assumed to be a cylinder [30], where the unloaded volume (V; equation 3) was determined using the unloaded outer radius (R_o), unloaded wall thickness (H), and the unloaded length (L). The unloaded geometry was used for both the active and passive state reference configuration but was determined separately for control and elastase-treatment conditions.

$$V = \pi(R_0^2 - (R_o - H)^2)L \quad \text{(Equation 3)}$$

Assuming the vagina behaves as an incompressible soft tissue, the deformed inner radius (r_i) was estimated (equation 4) based on the measured deformed length (l) and outer radius (r_o).

$$r_i = \sqrt{r_o^2 - \frac{V}{\pi l}} \quad \text{(Equation 4)}$$

The wall-averaged circumferential (σ_θ; equation 5) and longitudinal (σ_z; equation 6) Cauchy stresses were determined based on the deformed geometry (inner radius r_i and outer radius r_o) and the corresponding intraluminal pressure (P) and transducer-measured longitudinal force (F_t) [40, 46].

$$\sigma_\theta = \frac{Pr_i}{r_o - r_i} \quad \text{(Equation 5)}$$

$$\sigma_z = \frac{F_t + \pi P r_i^2}{\pi(r_o^2 - r_i^2)} \quad \text{(Equation 6)}$$

The circumferential stretch (λ_θ; equation 7) of the vagina in response to loading was calculated as the ratio of the deformed mid-wall radius to the unloaded mid-wall radius and the longitudinal stretch (λ_z; equation 8) was defined as the ratio of the deformed longitudinal length (l) to the unloaded longitudinal length (L).

$$\lambda_\theta = \frac{(r_i + r_o)/2}{(R_i + R_o)/2} \quad \text{(Equation 7)}$$

$$\lambda_z = \frac{l}{L} \quad \text{(Equation 8)}$$

Circumferential and longitudinal material stiffness values were calculated as the local tangent (slope) of the circumferential and longitudinal stress-stretch curves, respectively

(equation 9, equation 10). The slope was calculated by applying the MATLAB *polyfit* linear function to the region between the lower physiologic pressure boundary (LPB) and the upper pressure boundary (UPB). Pressure boundaries were defined as +/- one standard deviation away from the average balloon catheterization-measured physiologic pressure, as described in section 2.1 [22, 24].

$$Circumferential\ material\ stiffness = \frac{\sigma_\theta^{UPB} - \sigma_\theta^{LPB}}{\lambda_\theta^{UPB} - \lambda_\theta^{LPB}} \quad \text{(Equation 9)}$$

$$Longitudinal\ material\ stiffness = \frac{\sigma_z^{UPB} - \sigma_z^{LPB}}{\lambda_z^{UPB} - \lambda_z^{LPB}} \quad \text{(Equation 10)}$$

2.7 Ultrasound Imaging.

Vaginal wall thickness was determined ex vivo from cross-sectional ultrasound images acquired at the unloaded configuration in the control and elastase-treated conditions (Vevo2100 FUJIFILM VisualSonics Inc., Toronto, ON, Canada) using a 40MHz center frequency transducer (LZ550, resolution: 30 μm). Ultrasound images were obtained at the proximal region of the vagina due to similar portions of the vaginal wall being optically tracked during pressure-diameter testing. The longitudinal force and pressure were monitored to ensure stability and served as an indication that the tissue was not subjected to external compression during ultrasound assessment. The thickness of the vagina was measured in ImageJ (NIH, Bethesda, MD) by manually tracing 25 transmural lines around the tissue circumference [22, 47].

2.8 Immunofluorescence Imaging.

Following mechanical testing, the proximal half of the vagina (n=5/ group) was prepared for sectioning and staining. Samples were embedded in Tissue-Plus™ O.C.T. Compound (PANTeK Technologies, 23-730-571) at -80 °C prior to cryosectioning along the circumferential and longitudinal directions at an 8 μm section thickness (NX50 CryoStar). For immunostaining, O.C.T. was removed by washing in 1X phosphate buffered saline (PBS), and sections were fixed/permeabilized using a combined 10% neutral buffered formalin (Millipore Sigma, HT501128) and 0.1% Triton-X (Sigma-Aldrich, x100) solution. After fixation/permeabilization, sections were washed in PBS before blocking in a solution of 5% bovine serum albumin (Sigma-Aldrich, A3059) and 5% goat serum (Sigma-Aldrich, G9023) in PBS for 1 hour at room temperature. Samples were then stained at room temperature with a primary antibody against murine tropoelastin exons 6-17 [48, 84] (1:300 for 4 hours) followed by a mixture of Cy5 secondary antibody (Abcam, ab6564) and conjugated αSMA-Cy3 monoclonal antibody (Millipore Sigma, C6198) (both at 1:300 for 1 hour) and gentle rocking in PBS for 30 mins. Finally, samples were mounted in Prolong Gold with DAPI (Invitrogen, P36935) and immunofluorescent images were acquired on an Olympus BX53 microscope with an Olympus DP80 dual-sensor CCD camera using a 20X magnification objective. All images were acquired at the same exposure settings for consistent visual comparison. Quantification of elastin and smooth muscle area fraction analysis was performed using the image processing capabilities of FIJI (NIH) [85]. Determination of individual elastic fiber geometric properties (e.g., fiber length and fiber width) were determined using the open source MATLAB software package CT-FIRE [86].

2.9 Quantitative Polymerase Chain Reaction (qPCR).
Following mechanical testing, the distal half of each vaginal sample (n=5/ group) was prepared for RNA extraction and gene expression analysis. Total RNA was isolated after tissue homogenization (TissueLyser II) using the Qiagen RNeasy Micro Kit (Qiagen, 74004), and RNA yield for each sample was determined using a NanoDrop™ Spectrophotometer (Fisher Scientific, MA, USA). DNase I-treated RNA (1 ng per sample) was used for cDNA synthesis using SuperScript IV VILO Master Mix (Invitrogen, 11766050), and qPCR was performed using PowerTrack SYBR Green Master Mix (Invitrogen, A46012) in a QuantStudio3 Real-Time PCR system (ThermoFisher Scientific). Forward and reverse primers for contractile genes of interest (*Acta2*, *Actg*, and *Vim*) were designed (Integrated DNA Technologies, Iowa, USA). Comparison of multiple housekeeping genes revealed that Ct values for beta-actin (*Actb)* were the most consistent across age and elastase treatment. Therefore, gene expression was normalized to that of *Actb* in all comparisons. The forward and reverse primer sequences used in the current study were *Actb*: 5' CAGCCTTCCTTCTTGGGTATG 3' (forward) and 5' GGCATAGAGGTCTTTACGGATG 3' (reverse), *Acta2*: 5' TCTGGACGTACAACTGGTATTG 3' (forward*)* and 5' GGCAGTAGTCACGAAGGAATAG 3' (reverse), *Actg*: 5' CCGCCCTAGACATCAGGG 3' (forward*)* and 5' TCTTCTGGTGCTACTCGAAGC 3' (reverse), and *Vim*: 5' CTCGTCACCTTCGTGAATACC 3' (forward*)* and 5' TTGGCAGAGGCAGAGAAATC 3' (reverse). Following amplification, the relative expression of target genes was calculated using the $2^{-\Delta Ct}$ method [49]; for each gene, individual data points were then normalized by the geometric mean of the 2-3 months control gene expression.

2.10 Statistical Analysis.
A power analysis ($\beta = 0.80;\ \alpha = 0.050$) demonstrated that 8 samples were needed within each group to detect differences in mechanical properties with age and elastic fiber disruption. All other statistical analyses were performed by hypothesis using R (3.6.2); for all data presented in the manuscript, the error was normally distributed as determined by the Shapiro-Wilk test ($p>0.05$). Changes in the in vivo vaginal pressure with age were evaluated with a one-way ANOVA (age). Alterations in vaginal contractile potential were evaluated by one-way ANOVAs (age) comparing differences in the change in outer diameter and the change in longitudinal force with respect to age. Similarly, changes in vaginal microstructural composition were evaluated by one-way ANOVAs (age) comparing differences in elastin and αSMA area fractions with age. Multiple two-way ANOVAs (age, direction) examined differences in the maximum contractile stress of the vagina and direction-dependent differences in basal material stiffness with age. To determine the contribution of elastic fibers in the vaginal wall, multiple two-way ANOVAs (age, elastase) compared the circumferential and longitudinal contractile function in control and elastase samples with age. A two-way ANOVA (age, elastase) was also used to evaluate changes in normalized gene expression with respect to age and elastase treatment; statistical analysis of gene expression data was performed on the raw ΔCt values. Multiple three-way ANOVAs (age, direction, elastase) evaluated differences in the wall stress at maximum contraction and material stiffness before and after elastase treatment. To control for multiple comparisons, Tukey's post hoc HSD testing was performed when appropriate. In addition to groupwise comparisons, the Pearson

correlation coefficient r was used to evaluate linear relationships between normalized gene expression values ($2^{-\Delta Ct}$) and biaxial active mechanical properties. Finally, distributions of elastic fiber properties (e.g., length and width) were compared across age and elastase treatment by Kolmogorov–Smirnov (KS) testing and the descriptive metrics of skewness (symmetry) and kurtosis (tailedness). For all statistical comparisons, a value of $p<0.05$ was considered statistically significant with specific differences and correlation coefficients indicated in each figure. Data throughout the manuscript is presented as mean ± standard error of the mean, unless otherwise noted.

3. Results

3.1 Non-pregnant vaginal smooth muscle cell contractility was reduced with age.

To investigate age-dependent changes in vaginal smooth muscle cell (SMC) contractile function, the maximum change in outer diameter and longitudinal force was measured in response to vasoactive stimulation. Increasing age from 2-3 months to 10-14 months induced a progressive decrease in both the change in outer diameter ($p<0.001$; one-way ANOVA; Figure 1A) and the change in longitudinal force ($p<0.001$; one-way ANOVA; Figure 1B). Together, this suggests age reduced the biaxial contractile response of the non-pregnant murine vagina.

3.2 Reduced contractility was consistent with age-induced stiffening of the vagina.

In addition to geometric changes, the wall stress was calculated at maximum contraction as a normalized measure of force in the circumferential and longitudinal directions. Aging led to a progressive increase in the biaxial wall stress that was consistently higher in the circumferential direction compared to the longitudinal direction ($p<0.001$; two-way ANOVA (age, direction); Figure 1C). Multiple comparison testing (post-hoc Tukey's HSD) further demonstrated that the circumferential stress was greater than the longitudinal stress at 4-6 months ($p=0.026$), 7-9 months ($p=0.03$), and 10-14 months ($p=0.01$). Additionally, the stress was significantly greater at 7-9 months compared to 2-3 months in both the circumferential ($p=0.005$) and longitudinal ($p=0.003$) directions (Figure 1C). The increase in stress may be driven by a trend toward larger outer diameter during testing at maximum contraction ($p=0.09$; data not shown).

Cyclic pressurization and geometric assessment under basal conditions resulted in the generation of biaxial stress-stretch plots. Increasing age from 2-3 months to 10-14 months induced a progressive leftward shift in the stress-stretch responses in both the circumferential (Figure 2A) and longitudinal direction (Figure 2B) indicating a structural stiffening of the vaginal wall with age. Linearization of the nonlinear stress-stretch responses between upper and lower pressure bounds determined by balloon catheterization measurements (Figure 2C) was used to quantify biaxial material stiffness. Note that albeit increasing with age, pressure values were not found to be significantly different ($p=0.24$; one-way ANOVA; Figure 2C table). Material stiffness values progressively increased in both the circumferential (Figure 2D) and longitudinal direction (Figure 2E) and with age from 2-3 months to 10-14 months. Circumferential stiffness was consistently larger than the longitudinal stiffness at each age ($p<0.001$; two-way ANOVA (age, direction); Figure 2D,E). Material stiffness values showed significant interactions

between age and direction ($p<0.001$; two-way ANOVA) (Figure 2), therefore multiple comparison testing could not be reliably performed.

3.3 Aging induced microstructural reorganization of the vaginal extracellular matrix.

Microstructural organization of the smooth muscle and elastic fiber network within the vaginal wall was visualized by immunofluorescence staining and imaging. At 2-3 months of age, the vaginal wall exhibited a sparse elastic fiber network (red; Figure 3A; top row) throughout the subepithelium and a dense elastic fiber network aligned with αSMA^+ smooth muscle (yellow; Figure 3A; top row) in the muscularis and adventitia; little to no elastin staining was localized in the epithelium at any age. Additionally, staining for αSMA – an indicator of contractile SMCs – selectively indicated the location of the muscularis layer in the outer portion of the vaginal wall. Histological sectioning along the longitudinal (Figure 3A; first column) and circumferential direction (Figure 3A; second column) revealed a similar degree of SMC morphology and orientation, consistent with prior observations of multiple primary orientations of vaginal smooth muscle [50].

Compared to 2-3 months of age, older samples appeared to have a thickened vaginal wall with changes most evident in the epithelium, subepithelium, and adventitia (cf. 2-3 months vs. 7-9 months; Figure 3A; first row vs. third row). This observation was confirmed by quantitative vaginal cross-sectional area measurements from histological images ($p=0.009$; one-way ANOVA), wherein relative to 2-3 months samples, the median cross-sectional area was increased by 27%, 16%, and 72% in 4-6 months, 7-9 months, and 10-14 months samples, respectively (Figure 3D). Note that here we defined cross-sectional area as the total wall area minus the epithelium area to facilitate accurate area fraction calculations of constituents (e.g., αSMA and elastin) not expressed in the epithelial layer.

Despite the trend toward increasing total cross-sectional area, the fraction of wall containing αSMA^+ staining progressively decreased with age ($p<0.05$; one-way ANOVA; Figure 3E) with 10-14 months samples exhibiting a 41% decrease in αSMA^+ area fraction relative to 2-3 months. This suggests the increase in vaginal cross-sectional area is likely driven by layers other than the muscularis. In addition to age-induced alterations in the muscularis fraction of the vaginal wall, older samples also displayed qualitative changes in SMC morphology and density (green arrowheads; Figure 3B,C; Control) which may also contribute to the observed reductions in biaxial contractility of the vagina.

Interestingly, we observed that the vaginal elastin area fraction was less affected by age and did not vary considerably between the 2-3 months and 10-14 months groups ($p>0.05$; one-way ANOVA; Figure 3F). Despite similar overall amounts Eln^+ staining in the vaginal wall, we found that targeted tropoelastin immunostaining revealed qualitative visual differences in the elastic fiber network. Namely, sectioning along the circumferential direction revealed changes in elastic fiber length and more pronounced radial orientation of elastic fibers in the subepithelium (white stars; Figure 3B,C; top row). Taken together, this suggests that despite similar amounts of Eln^+ staining, the elastic fiber network experiences microstructural alterations with advancing age.

3.4 Changes in elastin fiber properties are associated with aging.

To further explore the changes in elastic fiber network architecture induced by age, we performed a more detailed fiber-based characterization and analysis of the Eln^+ immunostaining using the open source software package CT-FIRE. While CT-FIRE was originally developed to detect and analyze collagen fibers, here we have used it to detect elastic fibers and calculate simple geometric descriptors (e.g., length and width) of individual fibers (green overlay; Figure 4A) [87]. Distributions of the relative frequency of elastic fiber length (Figure 4B) and fiber width (Figure 4C) have been constructed for each age group. Between 3000 and 5000 individual fibers were detected and analyzed per group. To determine differences in fiber metric distributions relative to 2-3 months, we compared cumulative distributions and found significant differences in fiber length at 4-6 months ($p=0.023$; KS test) and 7-9 months ($p=0.0007$; KS test), but not 10-14 months. Similarly, there was a trend toward altered fiber width at 4-6 months ($p=0.085$; KS test) and differences at both 7-9 months and 10-14 months ($p<0.0001$; KS test).

In addition to differences across age, we also examined the shape of the fiber metric distributions. Fiber length distributions were highly positive-skewed suggesting that the majority of fibers were smaller than the median value (dashed lines) independent of age (Figure 4B), whereas fiber width distributions were more symmetric (Figure 4C). We also observed a decrease in the kurtosis of the fiber length distributions with increasing age suggesting a decrease in the number of fibers in the tails of the distribution (i.e., decrease in large fiber lengths) while fiber width kurtosis was similar across ages. Consistent with the observed changes in fiber geometry, we also observed an increase in the number of detected fibers per field of view with increasing age (i.e., 2-3 month: 623±57.5 fibers, 4-6 month: 683±117 fibers, 7-9 month: 608±88.8 fibers, 10-14 month: 736±42.8 fibers). The combination of more elastic fibers with decreased length and width suggests age induces microstructural alterations in the vaginal elastic fiber network that resemble excess fragmentation which may contribute to reduced smooth muscle contractility.

3.5 Age-related changes in vaginal contractility correlated with contractile gene expression.

To assess the relationship between active biomechanical properties of the vagina and SMC contractility, the relative expression of several known smooth muscle-related genes was measured by qPCR. In particular, expression for the contractile genes *Acta2* and *Actg*, as well as the synthetic gene *Vim*, were reduced with age (Figure S1) with lower expression at 10-14 months than 2-3 months (Figure 5A,B). Since this trend in gene expression was consistent with the measured mechanical data, a linear correlation analysis was performed and revealed strong negative correlations between contractile gene expression and measures of vaginal contractility over natural aging (Figure 5C). With loss of *Acta2* gene expression, there was a trend toward decreasing the change in longitudinal force ($r = 0.881$; Figure 5D) and increasing the change in outer diameter ($r = -0.912$; Figure 5E) and circumferential stress ($r = -0.931$; Figure 5F). Together, this contractile gene expression data supports the findings of altered tissue-level contractility with aging vaginal tissue.

3.6 Elastic fiber disruptions decreased contractility in younger mice.

To investigate if contractile potential of vaginal smooth muscle was affected by elastic fiber disruption, vaginal samples at 2-3 months, 4-6 months, 7-9 months, and 10-14 months of age were exposed to elastase treatment (Figure 6). Following elastase treatment, contractile assessment was performed and compared to age-matched control samples. The change in outer diameter significantly decreased in elastase samples aged 2-3 months ($p<0.001$; Figure 6A) and 4-6 months ($p=0.013$; Figure 6B) but was not statistically different between control and elastase at 7-9 months and 10-14 months (Figure 6C,D). The change in longitudinal force was significantly decreased at 2-3 months ($p<0.001$; Figure 5E), 4-6 months ($p<0.001$; Figure 6F), and the 7-9 months ($p=0.005$; Figure 6G) elastase samples relative to control; 10-14 months was not significantly different (Figure 6H). Calculation of the percent change in outer diameter (Figure S2A) and longitudinal force (Figure S2B) between control and elastase samples further revealed a greater contribution of elastin to contractility in young mice that diminished with age ($p<0.001$; one-way ANOVA; Figure S2). Together, this suggests elastin plays a larger contributing role to the contractile response in younger groups (2-3 month and 4-6 months) than in older groups (7-9 months and 10-14 months), which may be due to the loss of functional elastin and microstructural remodeling associated with natural aging (cf. Figure 3).

3.7 Changes in basal mechanics were consistent with the role of elastic fibers in vaginal contractility.

The maximum contractile wall stress was greater in the elastase treated samples as compared to the control group in the 2-3 months ($p<0.001$; two-way ANOVA) and 4-6 months ($p=0.009$; two-way ANOVA), but not at 7-9 months or 10-14 months (Figure S3). Additionally, stress-stretch responses in elastase treated samples were structurally stiffer (leftward shift) than control responses indicating reduced distensibility (circumferential direction) and extensibility (axial direction) at each age (Figure 6A-D). Using these stress-stretch responses, the calculated material stiffness values were larger in the circumferential direction than in the longitudinal direction at all age groups ($p<0.001$; two-way ANOVA) (Figure 7). When treated with elastase, the circumferential stiffness was increased only at 2-3 months ($p=0.004$; Figure 7E); the longitudinal material stiffness increased with age but was not significantly altered by elastase treatment (Figure 7E-H). A three-way ANOVA (age, direction, elastase) evaluated the hypotheses that the material stiffness of the vagina will behave in a direction-dependent manner and increase with age due to a decreased role of elastic fibers. This analysis determined the material stiffness increased with age ($p<0.001$), elastase treatment ($p<0.001$), and was greater in the circumferential direction ($p<0.001$). However, post-hoc multiple comparison analysis was not conducted due to a significant interaction between direction and elastase ($p<0.001$) and a potential statistical trend identified with the interaction between age and direction ($p=0.08$) (Figure 7E-H).

3.8 Elastic fiber disruption altered microstructural organization of the vaginal wall.

Following elastase treatment, the vaginal wall microstructure was altered relative to age-matched control samples. In particular, the elastic fiber network appeared to be disrupted in elastase-treated samples, as expected (Figure S4), with fiber-based image analysis showing a decrease in the number of detected elastic fibers (i.e., 2-3 month: 289±53.3

fibers, 4-6 month: 366±43.3 fibers, 7-9 month: 463±69.9 fibers, 10-14 month: 465±106 fibers after elastase treatment) per microscopic field of view, relative to control. Quantification of identified elastic fibers showed reduced fiber length (increased skewness; Figure S5B) and decreased fiber width (Figure S5C), relative to control. Elastase had a greater effect on reducing elastic fiber width ($p<0.0001$ at all ages; KS test) than on reducing fiber length ($p<0.0001$ for 4-6 months and 7-9 months only; KS test) which is consistent with observations of age-induced elastic fiber thinning [65, 66]. Although elastic fibers were still present in the tissues, elastase treatment lead to fragmentation of the elastic fiber network throughout the subepithelium (white stars; Figure 3B,C; bottom rows) and around the SMCs in the muscularis (white arrowheads; Figure 3B,C; bottom rows). Elastase also induced changes in the SMC morphology and density within the muscularis (green arrowheads; Figure 3B, C; bottom rows) which may contribute to the altered contractile response in the 2-3 month group following elastic fiber disruption. Despite local observations of microstructural remodeling, vaginal cross-sectional area and corresponding area fractions of αSMA and elastin were largely unaffected by elastase treatment (Figure S4B-D).

3.9 Contractile genes and biomechanical properties were weakly correlated after elastase.

Smooth muscle cell genes (*Acta2*, *Actg*, and *Vim*) were detected in elastase-treated samples and compared to vaginal biomechanical measures. While elastase treatment exacerbated the decrease in contractile gene expression, relative to control (Figure 5A,B, Figure S1), a linear correlation analysis revealed weak correlations with the corresponding biomechanical data (Figure S6). This is likely due to the fact that elastase treatment has a large detrimental impact on the vaginal biomechanical response independent of any changes in contractile gene expression. Further, this may suggest that while the biomechanical response is dependent on elastic fiber integrity, gene expression may not be as affected by elastase treatment. Interestingly, the synthetic smooth muscle gene *Vim* showed a stronger correlation with biomechanical metrics than *Acta2* and *Actg* following elastase treatment. Together, results from this study indicate the pivotal role of elastin and functional elastic fiber integrity in maintaining smooth muscle contractility and the active mechanical behavior of the vaginal wall.

4. Discussion

Overall, the study presented herein investigated the effect of age and elastic fiber disruption on vaginal contractility**.** The first objective of this study was to quantify the biaxial function of vaginal smooth muscle with age. We hypothesized that vaginal contractility would decrease with age, which was supported by significant decreases in the circumferential and longitudinal contractile potential in older groups (Figure 1). This is consistent with a decrease in the fraction of smooth muscle cells in the vaginal cross-sectional area (Figure 3) and a reduction in contractile gene expression as a result of aging (Figure 5). In support of this finding, the contractile strength of human pelvic floor skeletal muscle (levator ani) samples from women aged 18-89 years was negatively correlated with age [51]. While this previous study in human tissue determined contractility changes in the pre- and postmenopausal age range, the study presented herein has focused on investigating vaginal changes in mice aged 2-14 months, which

approximately equates to 18-62 years of age in humans. The decrease in contractile potential observed in the murine model used in the current study may be due to age-related microstructural remodeling, such as changes in smooth muscle content, organization, or contractile filament structure [52, 53]. In human vaginal samples from pre-and post-menopausal women aged 37-75 years, smooth muscle content decreased in patients with pelvic organ prolapse compared to non-prolapse controls [54, 55]. While these findings include additional pelvic floor pathologies, the findings include an association with decreased vaginal cellularity which may be multifactorial and related to either repetitive use, changes in intra-abdominal pressure, or chronic vaginal distension, all of which may be associated with age [55, 56]. While cellularity measurements were outside of the scope of this study, immunofluorescent staining revealed a change in smooth muscle organization with age (Figure 3). In human urethral tissue, age-related decline in urethral closure was associated with decreased smooth muscle density and organization [57]. This may suggest a potential relationship between dynamic smooth muscle organization with age and changes in smooth muscle function. Alternatively, the decrease in maximum vaginal contractile potential in the current study may be due to a change in smooth muscle contractile receptor expression, such as a decrease in adrenergic receptors. Adrenergic expression is altered with age, as demonstrated by decreased cardiac adrenergic receptors in mice aged 6 months as compared to 3 months [58]. Herein, a strong negative correlation was observed between contractile smooth muscle gene expression and vaginal smooth muscle contractility with age (Figure 3). While the effects of age on the expression of vaginal smooth muscle receptors is not well understood, the results observed herein are consistent with other smooth muscle organs, such as the gastrointestinal tract and vasculature wherein smooth muscle contractility and several corresponding receptors decrease with age [59, 60].

Here, we observed that basal material stiffness increased with age in both the circumferential and longitudinal directions (Figure 2). Similar vaginal material stiffening was observed with the loss of smooth muscle basal tone in the C57BL/6 mouse aged 3-6 months [22]. Increased basal material stiffness may suggest there is vaginal extracellular matrix remodeling or remodeling of the smooth muscle itself with age. As such, the age-related stiffening and reduction in maximum contractile potential may be due to smooth muscle cells adopting a more synthetic phenotype, which is consistent with our observations of reduced contractile gene expression. In the human umbilical cord, smooth muscle cells sense the stiffness of the extracellular matrix and are able to modulate towards a synthetic phenotype in response to matrix stiffening [61]. Further, aging is associated with an increased synthetic phenotypic gene expression within other soft tissues, such as the vasculature [62, 63]. Because basal tone is calculated through both active and passive contributions, which considers the role of smooth muscle and the extracellular matrix simultaneously, the increased basal material stiffness in the current study may also indicate alterations in the vaginal extracellular matrix. Similar material stiffening with age was observed in the nulliparous CD-1 mouse under passive conditions, a condition at which mechanical properties are dictated solely by the extracellular matrix [24]. While microstructural analysis was not included in the prior study, passive vaginal stiffening is likely due to changes in the primary load bearing extracellular matrix content and organization, such as collagen fiber undulation and elastic fiber disruption or

fragmentation [24]. Herein, immunofluorescence imaging revealed an alteration in elastic fiber density and composition (Figure 3 and Figure 4) as well as the organization of smooth muscle cells (Figure 3). Together, this may suggest changes in the extracellular matrix composition and active smooth muscle contraction play a key role in vaginal biomechanics throughout advanced aging.

The second objective of this study was to determine the direction-dependent relationship between elastic fibers and smooth muscle contractility with age. In support of this hypothesis, we found circumferential and longitudinal smooth muscle contractile potential in younger age-matched samples was decreased following elastic fiber disruption; the difference, however, was not significant in older samples (cf. Figure 6). In previous work, we found that contractile potential also decreased following elastase treatment in the longitudinal direction in the C57BL/6 murine vagina aged 3-6 months [22]. Although post-hoc statistical comparisons to determine the functional role of elastic fibers were not appropriate due to significant and trending interactions, immunofluorescence showed that elastase treatment caused changes in elastic fiber microstructure in the 2-3 month group but not at 10-14 months (Figure 3B,C and Figure 4). Additionally, once normalized, the percent change in contractility between the control and elastase treated samples decreased with age (Figure S2), suggesting a decreased functional contribution of elastic fibers to vaginal contractility with age [64]. Further, increased age in human studies is associated with decreased tissue elasticity, increased elastic fiber fragmentation, and elastic fiber thinning [65, 66]. While these elastic fiber changes are well documented in humans, it is important to note that the half-life of elastin is significantly longer than the murine lifespan (approximately 70 years) [67]. In most organs, elastic fiber production occurs during gestation with minimal synthesis in the adult body [68]. However, in the female reproductive system, it is suggested that elastic fiber production may occur outside gestational development and during menstruation, pregnancy, and postpartum remodeling [69-73].

Further, the direction-dependent basal material stiffness increased while the elastic fiber contribution to vaginal contractility decreased with age. Within each age group, elastic fiber disruption resulted in a leftward shift of the stress-stretch response, indicating a decrease in distensibility in the circumferential direction and extensibility in the longitudinal direction (Figure 7A-D). Additionally, the basal material stiffness increased following elastase treatment (Figure 7E-H). This leftward shift of the stress-stretch curves and increase in material stiffness following elastic fiber disruption may be due to the load being transferred to surrounding microstructural components within the vaginal wall following elastin degradation, such as collagen fibers. In arteries, it has been hypothesized that a decrease in smooth muscle function can transfer the mechanical load to other structural components of the vessel wall [74]. This hypothesis was supported with the use of multiphoton imaging (SHG) in the aortas of male rabbits, wherein collagen fibers in the longitudinal direction were more undulated compared to the radial direction, which suggested smooth muscle cells in the radial direction inhibited the deformation or undulation of collagen fibers [75]. While multiphoton imaging was outside the scope of the investigation performed herein, the previous findings may have implications for a

potential mechanism coupling smooth muscle and remodeling extracellular matrix components with age.

Additionally, while both the circumferential and longitudinal directions exhibited decreased distensibility and increased material stiffness following elastase treatment, the circumferential material stiffness was significantly greater than the longitudinal direction (Figure 6E-H). This may be due to direction-dependent microstructural composition and orientation. In the vagina of C57BL/6 mice, there was a higher elastin content in the longitudinal direction, as compared to the circumferential [22]. While formal direction-dependent microstructural composition quantification was outside the scope of this study, there is evidence to suggest the vagina contains microstructural components, such as smooth muscle cells and elastic fibers, in both the circumferential and longitudinal direction [20, 76-79]. As such, these components may remodel in a direction-dependent manner with age, thus resulting in the increased material stiffness that was observed in the circumferential direction.

The current study is not without limitations. While mice offer several benefits as an alternative model to fresh human samples, alterations in the hormonal mileiu with age in mice may differ from that of human women. Humans can spend approximately one-third of their life in peri- or postmenopausal states, characterized by acyclic menstrual cycles or low estrogen [80]. Mice do not become acyclic or exhibit low estrogen until 18-24 months, wherein they are termed “fully aged” and thereby do not directly mimic the physiology of human menopause [81]. Mice aged 8-10 months, however, undergo prolonged labor that closely mimics that observed in pregnancies of older women which may be a consequence of reduced vaginal contractile potential, microstructural alterations, and gene expression changes identified in the current study [82]. While the mouse model is associated with inherent limitations, previous findings and the work presented herein the mouse model offers a critical first step in elucidating the impact of age on the vaginal mechanical behavior while adjusting for variables such as parity and reproductive pathologies, such as prolapse. Additionally, pressure catheterization was conducted on anesthetized mice using 1-1.5% isoflurane in 100% oxygen. Throughout the experiment, anesthesia depth was carefully regulated to maintain a respiratory rate of approximately 1 breath per second. Despite pressure measurements showing no significant variance between the initial and final stages of the experiment, it's important to note that inherent biological variability in metabolism might introduce fluctuations in vaginal pressure measurements.

In the current study, RNA isolation, qPCR, and immunofluorescence analysis was performed on mechanically tested vaginal tissues in order to develop paired correlations with biomechanical measurements. We found that this approach led to a reduction in the quality and quantity of RNA relative to non-tested samples but did not preclude gene expression analysis altogether. However, this may have contributed to the variance in gene expression we found within age/treatment groups. In our experience, mechanical testing does not have a pronounced effect on soft tissue ECM structure and organization. Thus, we expect minimal impact of mechanical testing on our immunofluorescence quantification. Previous work in the non-tested CD-1 mouse used immunoimaging

techniques to quantify uterine epithelium thickness with pharmaceutical regimes [83]. However, baseline immunostaining characterization of the CD-1 vagina remains unknown. Given the purpose of this study was to provide preliminary observations into the vaginal microstructural composition with age, our combination of qualitative and quantitative immunostaining and qPCR analysis – albeit in mechanically-tested tissues – provided a reasonable first step towards understanding the dynamic changes in vaginal microstructural with age. Additional studies are needed to compare results from the murine model to data generated from human or cadaveric samples to better understand the microstructural processes responsible for changes in mechanical properties with age, as well as to better inform clinical practices regarding age-related pathologies, such as pelvic organ prolapse or maternal injuries during birth.

6. Conclusion

In summary, age was associated with decreased vaginal contractility, increased material stiffness under basal tone, alterations in vaginal wall composition, and was negatively correlated with contractile gene expression. Additionally, elastic fiber disruption resulted in decreased contractility and alterations in vaginal wall composition in younger mice that was less apparent in older mice. Together, this emphasizes that elastic fiber disruption may contribute to decreased vaginal smooth muscle contractility and suggests a decreased functional role of elastic fibers with age. The findings presented herein provide a first step in understanding the dynamics between biomechanical function, microstructure, and age.

FUNDING

The NSF Award no.1947770 (K.S.M) and NSF Award no. 2326797 funded this work.

ACKNOWLEDGMENTS

We acknowledge Dr. Carolyn Bayer and Dr. Dylan Lawrence for training personnel on ultrasound use techniques and access to the Vevo 2100 Ultrasound system.

Figures

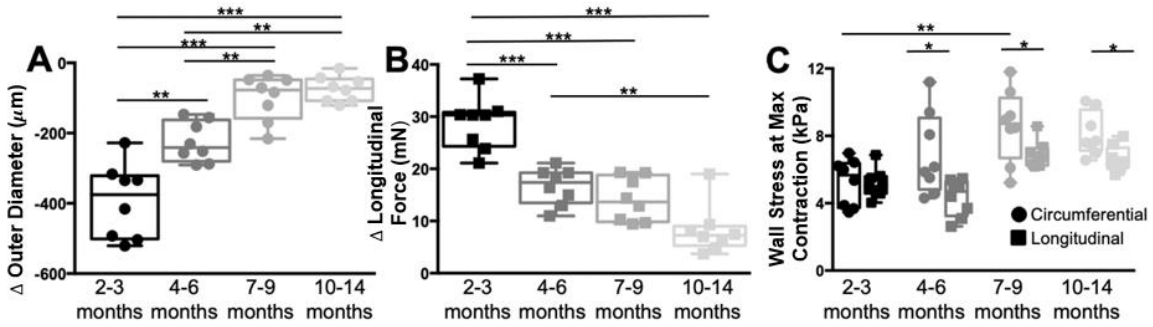

Figure 1. The circumferential and longitudinal contractile potential of the vagina decreases with age. A one-way ANOVA (age) determined that the change in outer diameter (circumferential contractile potential; circle) significantly decreased with increasing age ($p<0.001$) (A). An additional one-way ANOVA observed (age) a significant decrease in the change in longitudinal force (axial contractile potential; squares) with increasing age ($p<0.001$) (B). Additionally, a two-way ANOVA (age: direction) evaluated the maximum vaginal wall stress when stimulated with potassium chloride in the circumferential (circle) and longitudinal (square) direction (C). Contractile stress significantly increased with age ($p<0.001$) and was greater in the circumferential direction ($p=0.001$). Tukey Post Hoc tests demonstrated significant differences between directions in the 4-6 months (dark grey; $p=0.026$), 7-9 months (grey; $p=0.03$), and 10-14 months (light grey; $p=0.01$) groups. Additionally, the wall stress at maximum contraction increased with age, as demonstrated by significant differences in the 7-9 months compared to the 2-3 months in both the circumferential ($p=0.005$) and longitudinal ($p=0.003$) direction. Data represents n=8/ group.

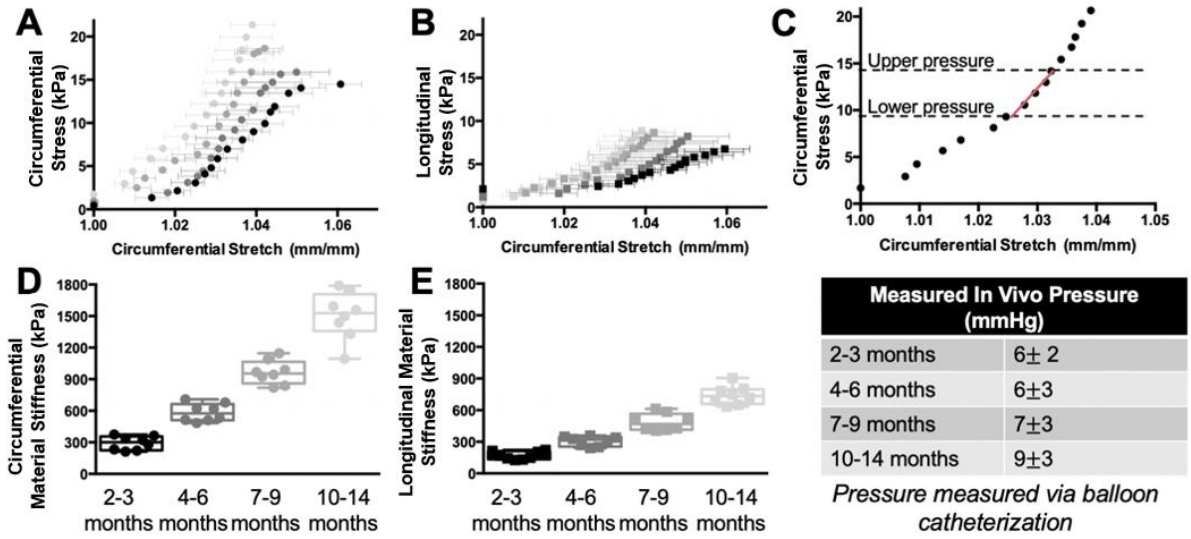

Measured In Vivo Pressure (mmHg)	
2-3 months	6± 2
4-6 months	6±3
7-9 months	7±3
10-14 months	9±3

Pressure measured via balloon catheterization

Figure 2. The basal circumferential and longitudinal material stiffness of the vagina increases with age. Increasing age in the 4-6 months (dark grey), 7-9 months (grey) and 10-14 months (light grey) resulted in a progressive leftward shift of the stress-stretch curves (decreased distensibility) as compared to the 2-3 months (black) in both the circumferential (A; circles) and longitudinal (B; squares) directions. The material stiffness in both the circumferential and longitudinal directions was determined by fitting a linear function through the stress-stretch curve between the upper and lower pressure bound, as determined by balloon catheterization (C). A one-way ANOVA determined the in vivo pressure did not significantly differ with age ($p=0.24$). The circumferential (D) and longitudinal (E) material stiffness increased with age ($p<0.001$) and was greater in the circumferential direction ($p=0.008$). Post-hoc multiple comparison tests were not conducted due to a significant interaction between age and direction ($p=0.044$). n = 8 per age group.

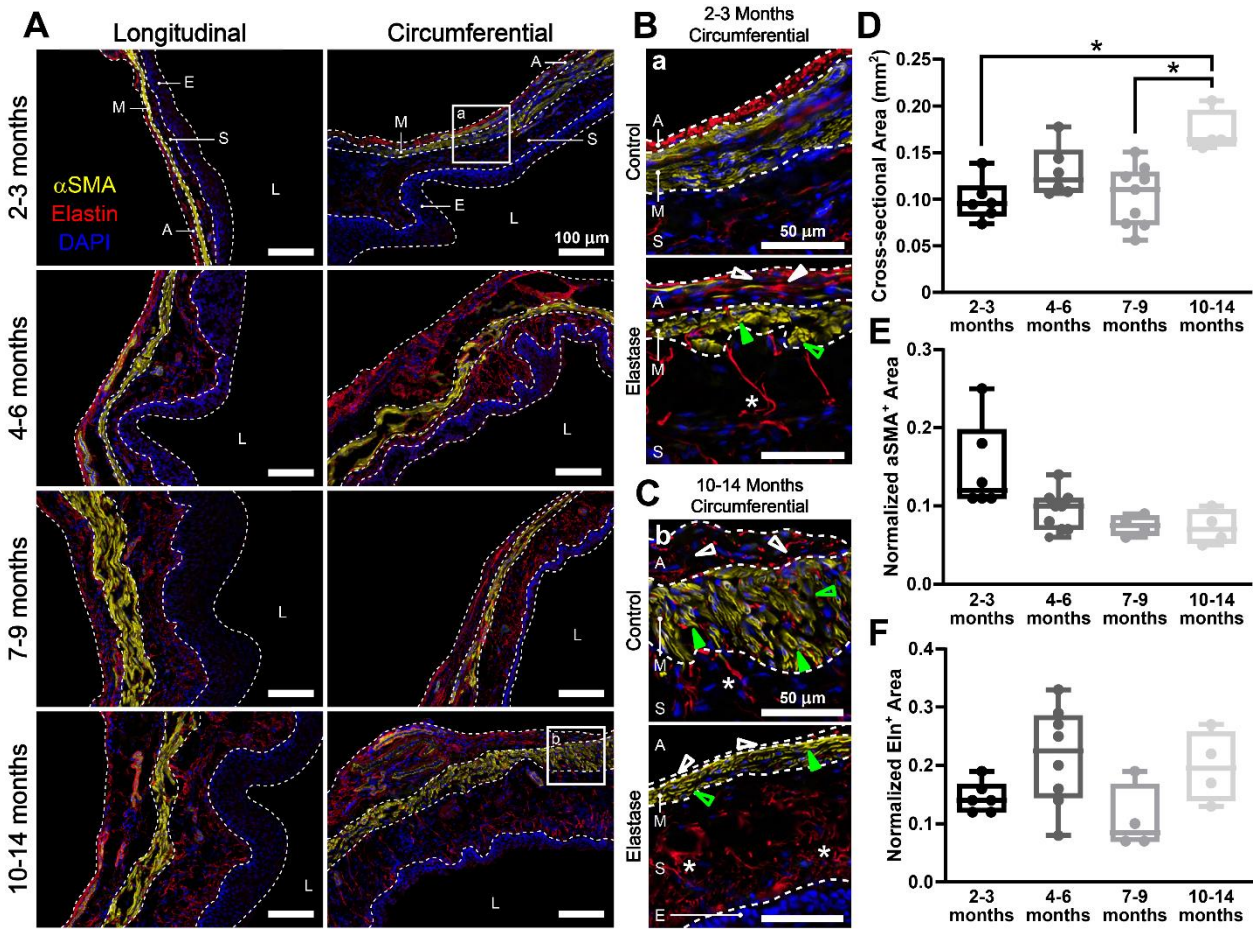

Figure 3. Vaginal wall composition is altered by both age and elastase treatment. Immunofluorescent labeling of alpha-smooth muscle actin (yellow; αSMA), elastin (red), and cell nuclei (blue; DAPI) revealed the microstructural organization within the vaginal from 2-3 months to 10-14 months of age (A; rows). Sectioning was performed along the circumferential and longitudinal directions for comparison (A; columns). Dashed lines indicate the borders of the vaginal lumen (L), epithelium (E), subepithelium (S), muscularis (M), and adventitia (A). Higher magnification histological observations (inset panels a and b) indicated changes in elastic fiber structure (B,C; open white arrowhead) with both age (B,C; first row) and elastase treatment (B,C; second row); elastase further altered elastic fiber structure (B,C; closed white arrowhead) in the adventitia and subepithelium. All groups exhibited changes in elastic fiber morphology (B,C; white star) compared to 2-3 months control. Changes in smooth muscle cell orientation (B; solid green arrowhead) and density (B,C; open green arrowhead) were also observed with both aging and elastase treatment. Scale bars are shown as either 100 μm (in A) or 50 μm (in B,C), as indicated. Quantification of vaginal cross-sectional area (total wall minus epithelium) was measured from histological images (D) and used to calculate the normalized area fraction of αSMA$^+$ staining (E) and elastin$^+$ staining (F) in each age group. * $p<0.05$, one-way ANOVA with post-hoc Tukey's HSD test. (D-F) n = 4-8 samples per group.

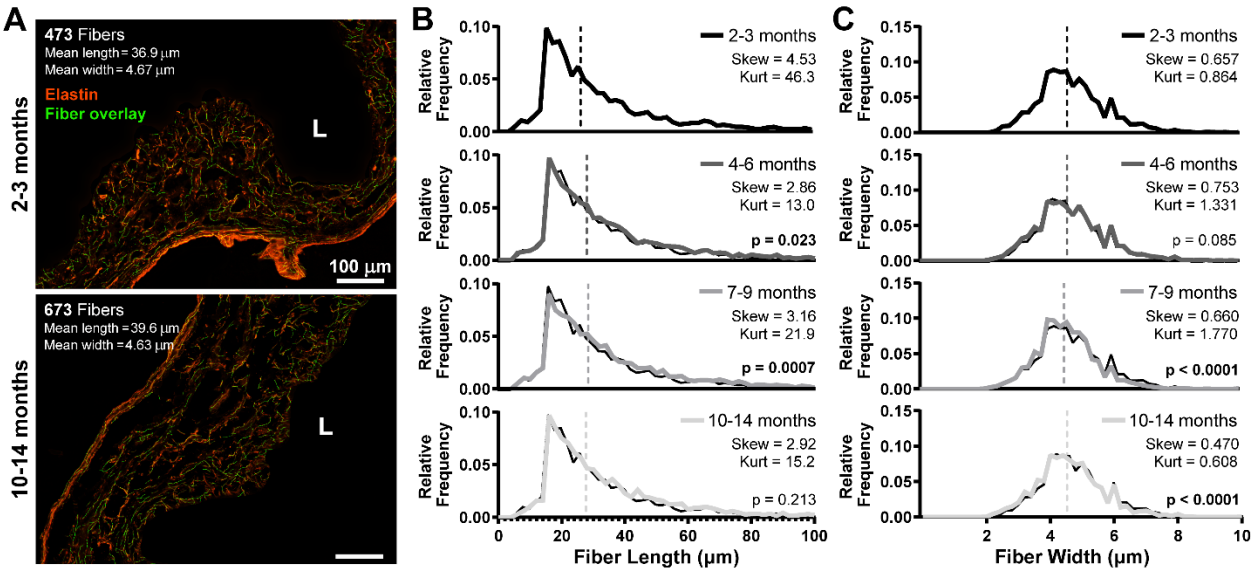

Figure 4. Vaginal elastic fiber structure is altered with age. Images containing immunofluorescent labeling of elastin (red) were processed with CT-FIRE to identify and extract geometric descriptors from individual elastic fibers (green overlay) in the vaginal wall (A). The vaginal lumen is denoted by L and scale bars are 100 μm. Changes in elastic fiber microstructural organization were assessed by measurement of fiber length (B) and fiber width (C) from 2-3 months to 10-14 months of age. The relative frequency (number of fibers of a given size divided by total number of fibers) was used to visualize distributions of fiber metrics; dashed lines denote median values. Note the high skewness of fiber length distributions (B) and the near symmetric fiber width distributions (C) independent of age. Changes in the descriptive statistics of each identified distribution suggest a reduced fiber length with age (decreased kurtosis and skewness); similar, albeit less pronounced, changes were observed in fiber width distributions. Statistical differences relative to the 2-3 month distribution (B,C; top row and black inset behind each distribution) were assessed by comparing cumulative distribution functions via the KS test; p values for each comparison are indicated.

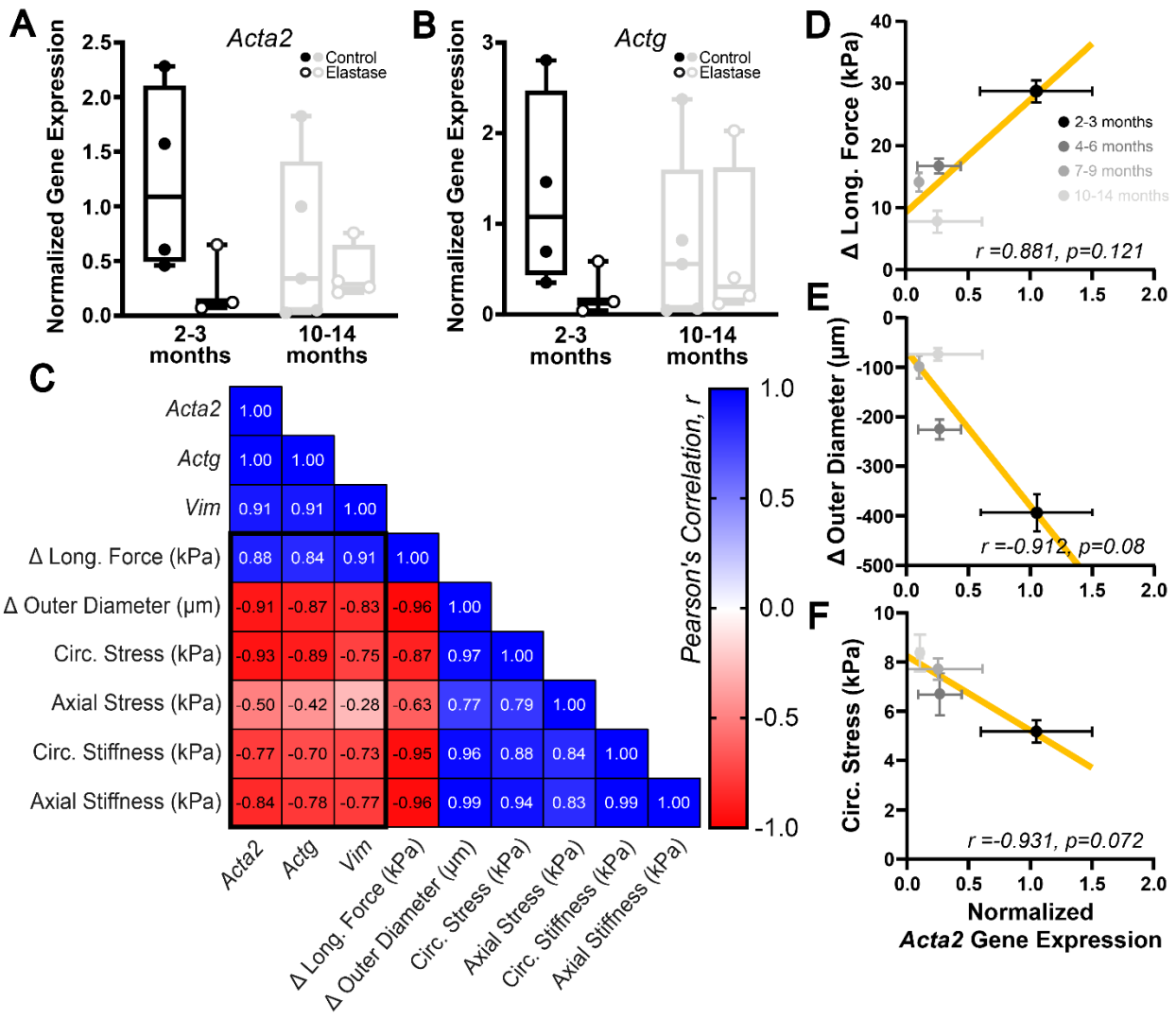

Figure 5. Vaginal contractility correlates with contractile gene expression. Normalized expression of smooth muscle contractile genes *Acta2* (A) and *Actg* (B) in the distal vagina showed a trend toward decreased median expression from 2-3 months to 10-14 months of age (filled circles) that was exacerbated following elastase treatment (open circles). Linear correlation analysis revealed a strong negative correlation (red squares) between measured smooth muscle genes (*Acta2*, *Actg*, and *Vim*) and active biaxial properties (loads, stress, and material stiffness) of the vaginal wall with age (C). Inset numerical values indicate correlation coefficients between variables. Illustrative comparisons between mechanical metrics and *Acta2* gene expression revealed a strong positive correlation with longitudinal force change (D; r = 0.881) and strong negative correlations with both outer diameter change (E; r = -0.912) and active circumferential stress (F; r = -0.931) with age. n = 3-5 per group for gene expression data and n = 8 per group for biaxial mechanical data; error bars indicate SEM. Correlation strength was evaluated by the Pearson correlation coefficient with r and p values denoted for each correlation.

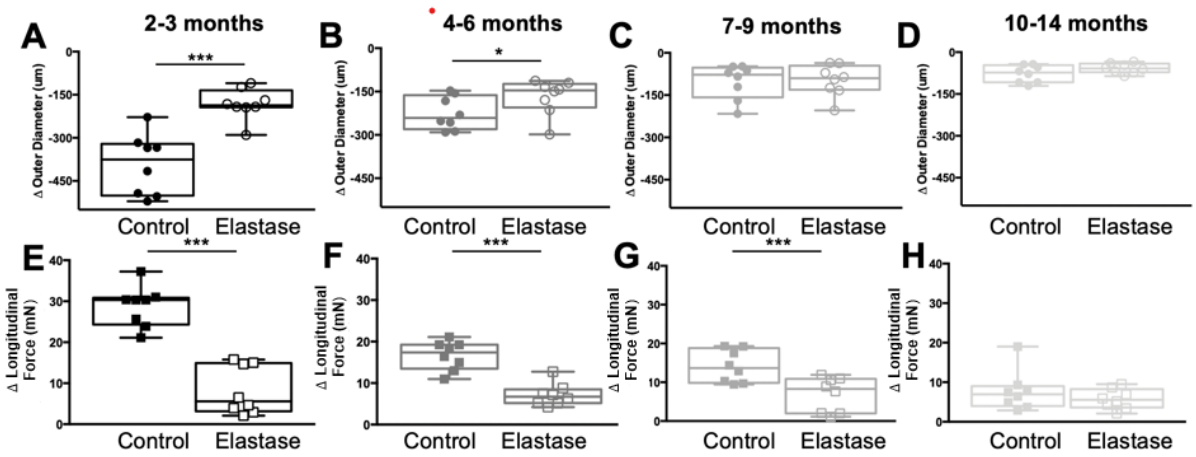

Figure 6. Circumferential and longitudinal contractile potential of the vagina decreased in an age-dependent manner following elastase treatment. To determine if the contractile potential was altered by elastic fiber disruption, t-test comparisons were completed for age-matched control (filled) and elastase-treated (outlined) samples. The change in outer diameter (circles) significantly decreased in elastase samples aged 2-3 months (A; black; $p<0.001$) and 4-6 months (B; dark grey; $p=0.013$), but not in 7-9 months and 10-14 months. The difference in longitudinal force (squares) significantly decreased in the 2-3 months (E; black; $p<0.001$), 4-6 months (F; dark grey; $p<0.001$), as well as the 7-9 months (G; grey; $p=0.005$). n = 8 per age group.

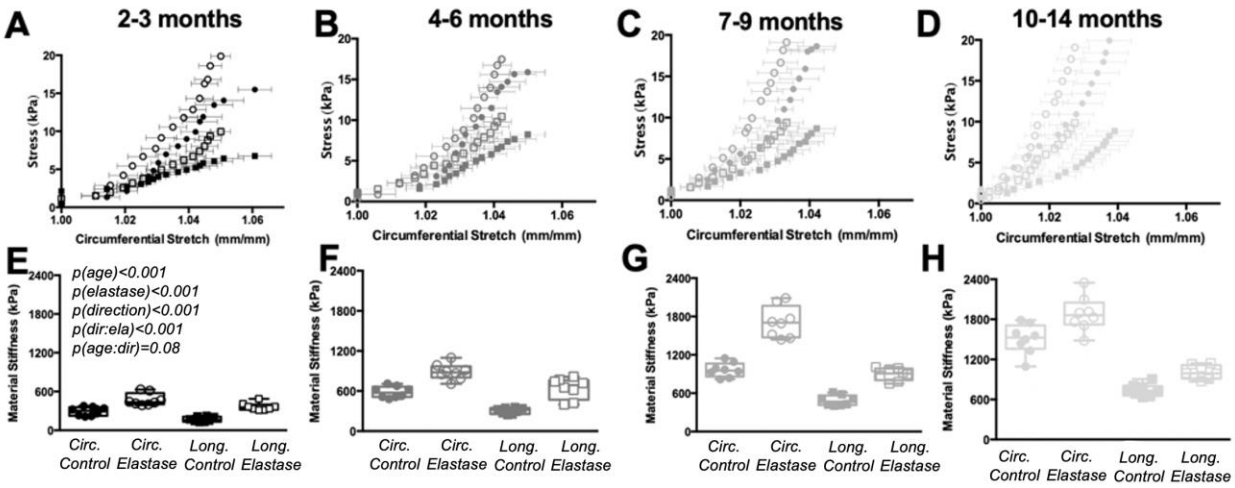

Figure 7. Elastase treatment resulted in a decrease in vaginal distensibility and increase in basal material stiffness. Elastase treatment (open markers) resulted in a consistent leftward shift in the biaxial stress-stretch responses indicating a decreased distensibility in the circumferential direction (circle) and decreased extensibility in the longitudinal (long.) direction (square) in mice aged 2-3 months (A, black), 4-6 months (B, dark grey), 7-9 months (C, grey), and 10-14 months (D, light grey). Using a three-way ANOVA (age, direction, elastase), the basal material stiffness was found to be increased with age ($p<0.001$) and elastase treatment ($p<0.001$) and was greater in the circumferential direction ($p<0.001$; E-H). Posthoc tests were not performed due to significant and trending interactions between direction and elastase ($p<0.001$) and age and direction ($p=0.080$).

SUPPLEMENTAL FIGURES

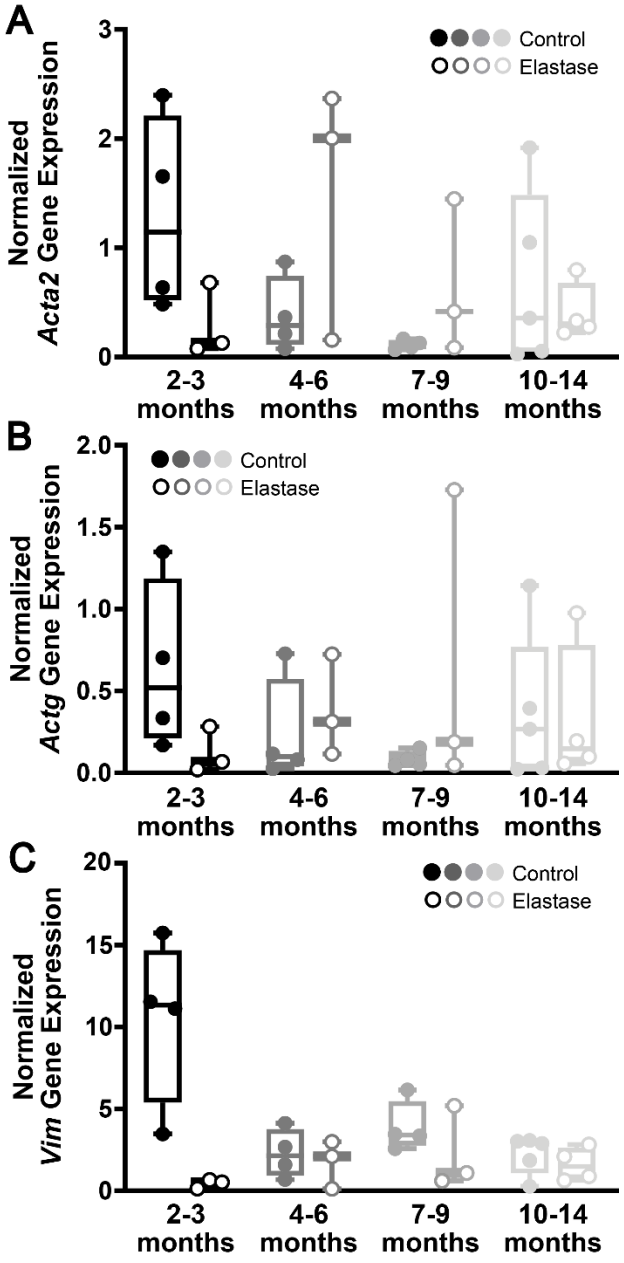

Figure S1. Contractile gene expression in the vagina with age and elastase treatment. Normalized relative expression of several known smooth muscle-related genes was assessed in the distal vagina of mice after aging from 2-3 months to 10-14 months of age (filled) and age-matched elastase treatment (open). Expression of *Acta2* (A), *Actg* (B), and *Vim* (C) was determined by qPCR; values were computed relative to the known housekeeping gene beta-actin (*Actb*) and normalized to the 2-3 months Control expression for each gene. +++Note the general trend toward decreasing contractile gene expression with increasing age and the further reduction following elastase treatment. n = 3-5 per group.

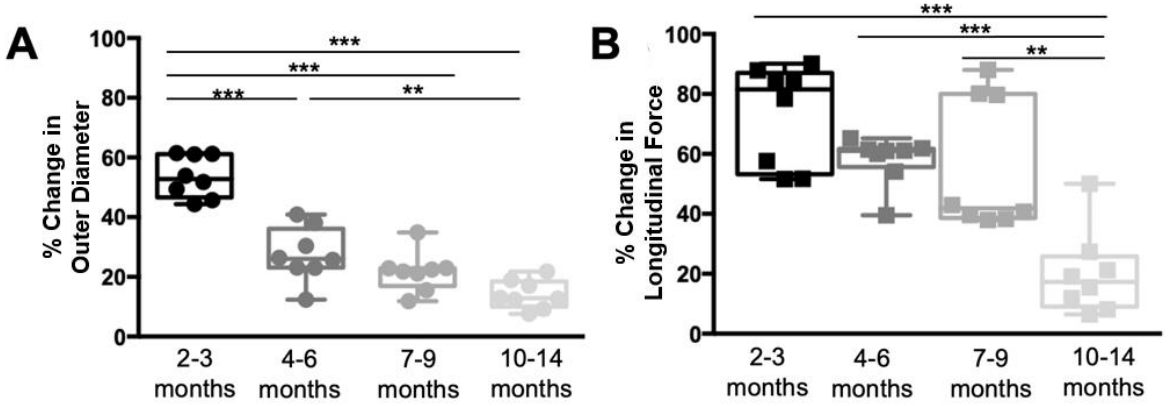

Figure S2. The contribution of elastic fibers to smooth muscle contractility is diminished with age in the circumferential and longitudinal directions. To quantify the contribution of elastic fibers on smooth muscle contractility, the percent change in circumferential contractile potential (A, circles), longitudinal contractile potential (B, squares) was calculated from the contractile responses before and after elastic fiber disruption. As determined by a one-way ANOVA (age), the percent change in circumferential contractile potential between control and elastase treated samples significantly decreased with age ($p<0.001$; A). Posthoc analysis identified the percent change in outer diameter was significantly reduced at 4-6 months ($p<0.001$), 7-9 months ($p<0.001$), and 10-14 months ($p<0.001$) as compared to the 2-3 months (A). Additionally, the percent change at 10-14 months was significantly less than at 4-6 months ($p=0.003$) (A). An additional one-way ANOVA (age) determined the percent change in longitudinal contractile potential was decreased with age ($p<0.001$; B). Further posthoc analysis identified a significantly lower percent change at 10-14 months as compared to the 2-3 months ($p<0.001$), 4-6 months ($p<0.001$), and 7-9 months ($p=0.006$), suggesting a greater effect of elastic fibers on vaginal contractility in younger mice than in older mice.

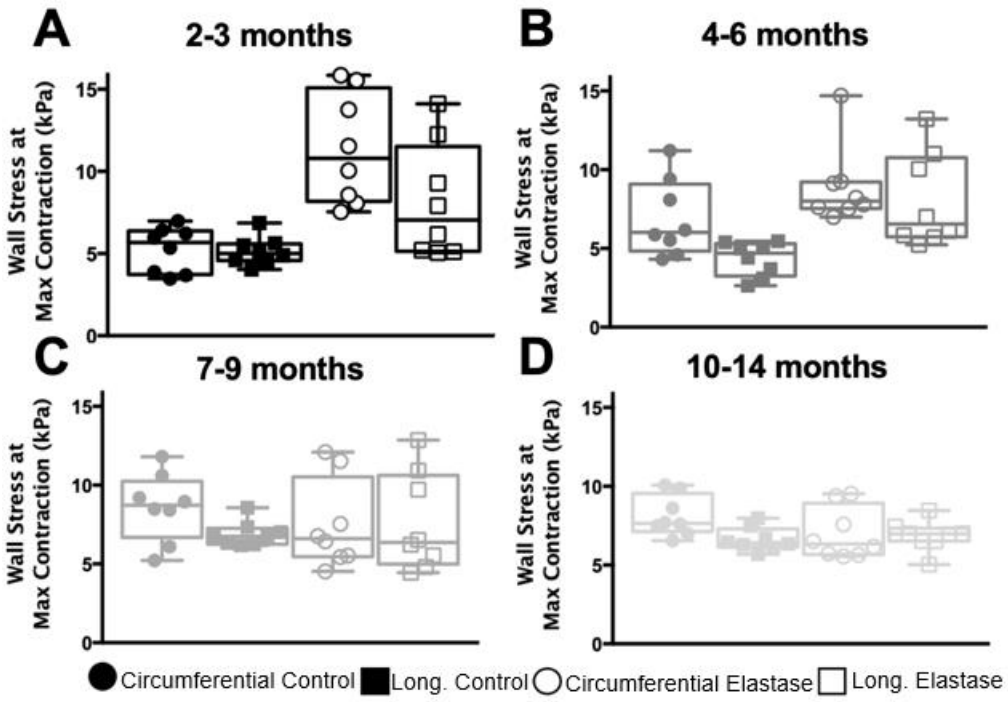

Figure S3. Vaginal wall stress during maximum contraction increased with age and elastic fiber disruption. A three-way ANOVA (age, direction, elastase) evaluated the potential differences in vaginal wall stress during maximum contraction in the circumferential (circle) and longitudinal (long.) (square) direction for the control (filled) and elastase-treated (open) samples aged 2-3 months (A, black), 4-6 months (B, dark grey), 7-9 months, (C, grey), and 10-14 months (D, light grey). The wall stress during contraction increased with age ($p<0.001$) and elastase treatment ($p=.03$). Posthoc tests were not completed due to significant and trending interactions between age and elastase treatment ($p=.04$) as well as age and direction ($p=0.07$).

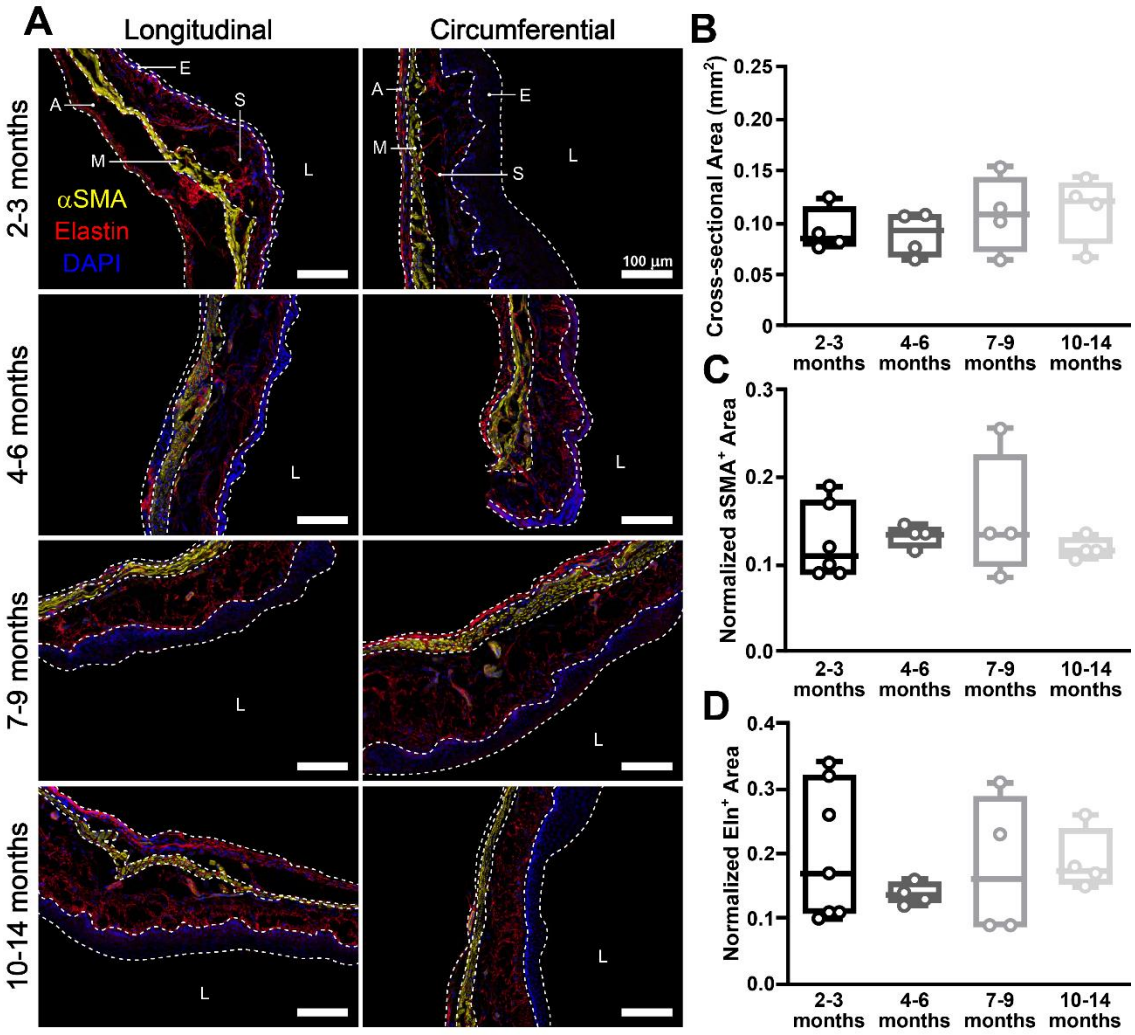

Figure S4. Immunofluorescent labeling of alpha-smooth muscle actin (yellow; αSMA), elastin (red), and cell nuclei (blue; DAPI) revealed the microstructural organization within the vagina treated with elastase at 2-3 months to 10-14 months of age (A; rows). Note the differences in elastin and smooth muscle organization between groups. Sectioning was performed along the circumferential and longitudinal directions for comparison (A; columns). Dashed lines indicate the borders of the vaginal lumen (L), epithelium (E), subepithelium (S), muscularis (M), and adventitia (A). Scale bars are 100 μm. Quantification of vaginal cross-sectional area (total wall minus epithelium) was measured from histological images (B) and used to calculate the normalized fraction of αSMA^+ area (C) and elastin$^+$ (Eln^+) area (D) as an additional measure of microstructural changes in each age group. Boxes denote the median and inter-quartile range of measurements in each age group. One-way ANOVA analysis revealed that neither cross-sectional area ($p=0.34$), nor normalized $aSMA^+$ ($p=0.35$) or Eln^+ ($p=0.82$) areas where siginificantly different with increasing age. (B-D) n = 4-8 samples per group.

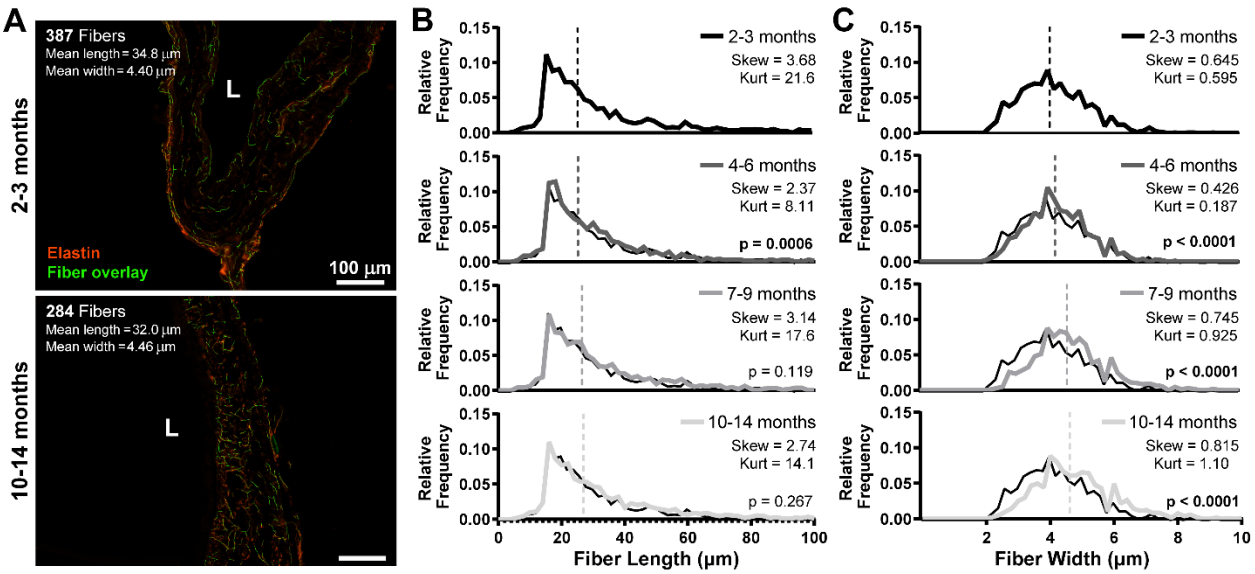

Figure S5. Vaginal elastic fiber structure is altered with age and elastase treatment. Images containing immunofluorescent labeling of elastin (red) were processed with CT-FIRE to identify and extract geometric descriptors from individual elastic fibers (green overlay) in the elastase-treated vaginal wall (A). The vaginal lumen is denoted by L and scale bars are 100 μm. Changes in elastic fiber microstructural organization were assessed by measurement of fiber length (B) and fiber width (C) from elastase-treated samples at 2-3 months to 10-14 months of age. The relative frequency (number of fibers of a given size divided by total number of fibers) was used to visualize distributions of fiber metrics; dashed lines denote median values. Note the high skewness of fiber length distributions (B) and the near symmetric fiber width distributions (C) independent of age. Comparisons with aging Control samples (cf. Figure 4 in the main text) can be used to assess the impact of elastase on elastic fiber geometry. In general, elastase has a strong effect on fiber width and a less pronounced effect on fiber length, suggesting it may contribute to elastic fiber thinning. Statistical differences relative to the 2-3 month distribution (B,C; top row and black inset behind each distribution) or age-matched untreated Controls (Figure 4B,C) were assessed by comparing cumulative distribution functions via the KS test; p values for each comparison are indicated or described in the Results section of the main text.

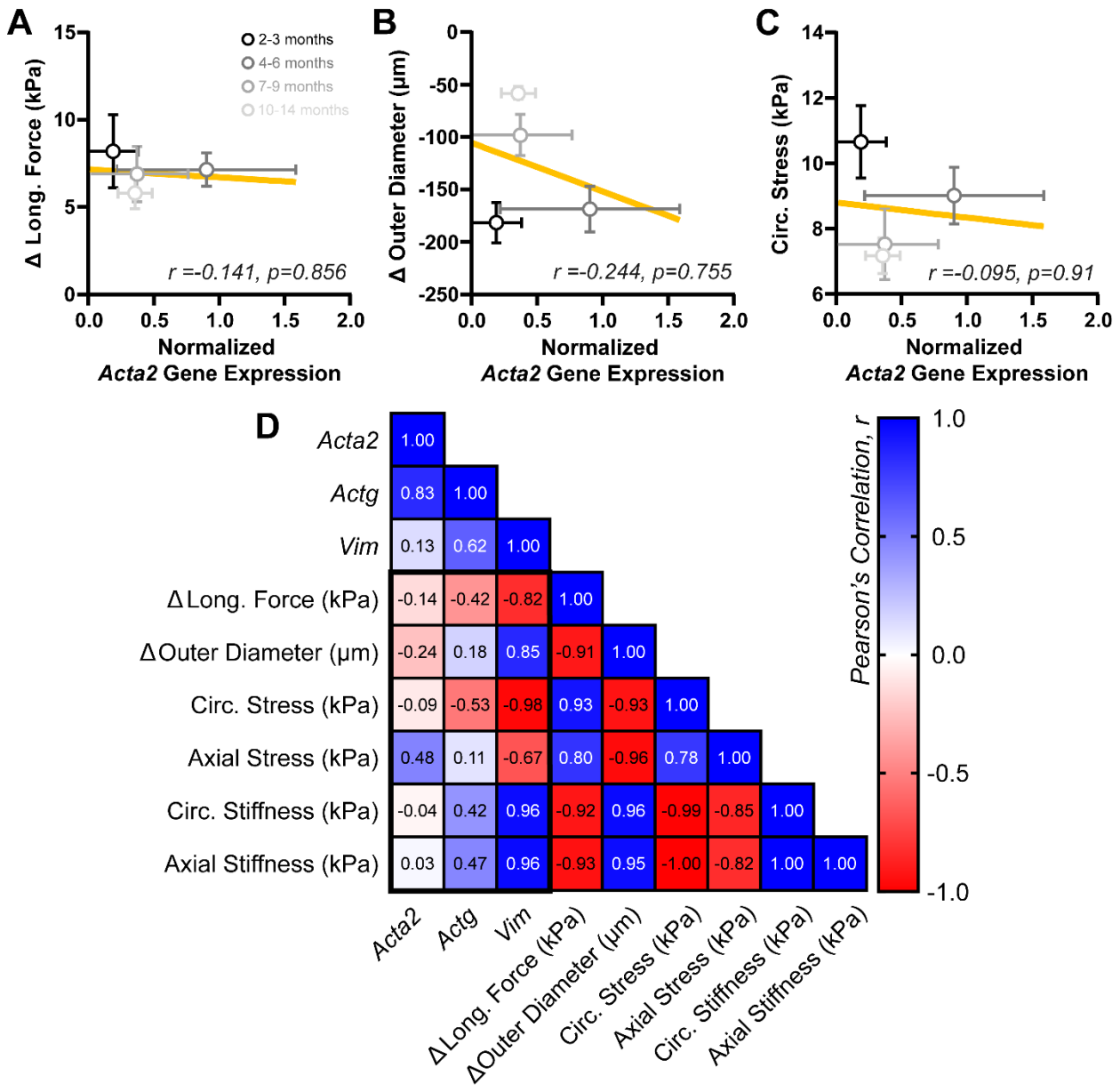

Figure S6. Vaginal contractility is reduced independent of contractile gene expression following elastase treatment. Illustrative comparisons between mechanical metrics and *Acta2* gene expression revealed weak negative correlations with longitudinal force change (A), outer diameter change (B), and maximum contractile circumferential stress (C) with age following elastase treatment. Linear correlation analysis revealed weak correlations between several contractile genes (*Acta2* and *Actg*) and active biaxial properties (loads, stress, and stiffness) of the vaginal wall following elastase treatment (C); *Vim* showed stronger correlations with mechanical metrics. Inset numerical values indicate correlation coefficients between variables. n = 3-4 per group for gene expression data and n = 8 per group for biaxial mechanical data; error bars indicate SEM. Correlation strength was evaluated by the Pearson correlation coefficient with r and p values denoted for each correlation.

References

[1] J.O.L. Delancey, Anatomie aspects of vaginal eversion after hysterectomy, American Journal of Obstetrics and Gynecology 166(6) (1992) 1717-1728.
[2] P. Rahmanou, J. Caudwell-Hall, I. Kamisan Atan, H.P. Dietz, The association between maternal age at first delivery and risk of obstetric trauma, American Journal of Obstetrics and Gynecology 215(4) (2016) 451.e1-451.e7.
[3] T.P. Matthews, C. Zhang, D.-K. Yao, K. Maslov, L.V. Wang, Label-free photoacoustic microscopy of peripheral nerves, Journal of biomedical optics 19(1) (2014) 16004.
[4] P.M.D.M. Rahmanou, J.M.D. Caudwell-Hall, I.M.D. Kamisan Atan, H.P.P. Dietz, The association between maternal age at first delivery and risk of obstetric trauma, American journal of obstetrics and gynecology 215(4) (2016) 451.e1-451.e7.
[5] T.T. Lao, L.-F. Ho, B.C.P. Chan, W.-C. Leung, Maternal age and prevalence of gestational diabetes mellitus, Diabetes care 29(4) (2006) 948-949.
[6] R. Gaillard, R. Bakker, E.A.P. Steegers, A. Hofman, V.W.V. Jaddoe, Maternal Age During Pregnancy Is Associated With Third Trimester Blood Pressure Level: The Generation R Study, American journal of hypertension 24(9) (2011) 1046-1053.
[7] A. Lethaby, R.O. Ayeleke, H. Roberts, Local oestrogen for vaginal atrophy in postmenopausal women, The Cochrane database of systematic reviews 2016(8) (2016) CD001500.
[8] C. Castelo-Branco, M.J. Cancelo, J. Villero, F. Nohales, M.D. Juliá, Management of post-menopausal vaginal atrophy and atrophic vaginitis, Maturitas 52(1) (2005) 46-52.
[9] J. Ferruzzi, M. Collins, A. Yeh, J. Humphrey, Mechanical assessment of elastin integrity in fibrillin-1-deficient carotid arteries: implication for Marfan syndrome, Cardiovascular Research 92(2) (2011) 287-295.
[10] K. Park, I. Goldstein, C. Andry, M. Siroky, R. Krane, K. Azadzoi, Vasculogenic female sexual dysfunction: the hemodynamic basis for vaginal engorgement insufficiency and clitoral erectile insufficiency, International Journal of Impotence Journal 9(1) (1997) 27-37.
[11] A. Feola, P. Moalli, M. Alperin, R. Duerr, R. Gandley, S. Abramowitch, Impact of Pregnancy and Vaginal Delivery on the Passive and Active Mechanics of the Rat Vagina, The Journal of the Biomedical Engineering Society 39(1) (2011) 549-558.
[12] L.C. Skoczylas, Z. Jallah, Y. Sugino, S.E. Stein, A. Feola, N. Yoshimura, P. Moalli, Regional Differences in Rat Vaginal Smooth Muscle Contractility and Morphology, Reproductive Sciences 20(4) (2013) 382-390.
[13] C. Jean-Charles, C. Rubod, M. Brieu, M. Boukerrou, J. Fasel, M. Cosson, Biomechanical properties of prolapsed or non-prolapsed vaginal tissue: impact on genital prolapse surgery, Including Pelvic Floor Dysfunction 21(12) (2010) 1535-1538.
[14] A. Feola, R. Duerr, P. Moalli, S. Abramowitch, Changes in the rheological behavior of the vagina in women with pelvic organ prolapse, Including Pelvic Floor Dysfunction 24(7) (2013) 1221-1227.
[15] G. Northington, M. Basha, L. Arya, A. Wein, S. Chacko, Contractile Response of Human Anterior Vaginal Muscularis in Women With and Without Pelvic Organ Prolapse, Journal of Reproductive Science 18(3) (2011) 296-303.
[16] M.L. Bochaton-Piallat, F. Gabbiani, P. Ropraz, G. Gabbiani, Age influences the replicative activity and the differentiation features of cultured rat aortic smooth muscle cell populations and clones, Arteriosclerosis and thrombosis 13(10) (1993) 1449-1455.
[17] J. Kruger, L. Hayward, P. Nielsen, D. Loiselle, R. Kirton, Design and development of a novel intra-vaginal pressure sensor, INTERNATIONAL UROGYNECOLOGY JOURNAL 24(10) (2013) 1715-1721.
[18] K.K. O'Dell, A.N. Morse, S.L. Crawford, A. Howard, Vaginal pressure during lifting, floor exercises, jogging, and use of hydraulic exercise machines, International Urogynecology Journal 18(12) (2007) 1481-1489.
[19] J.M. Shaw, N.M. Hamad, T.J. Coleman, M.J. Egger, Y. Hsu, R. Hitchcock, I.E. Nygaard, Intra-abdominal pressures during activity in women using an intra-vaginal pressure transducer, Journal of sports sciences 32(12) (2014) 1176-1185.
[20] A. Huntington, E. Rizzuto, S. Abramowitch, Z. Prete, R. De Vita, Anisotropy of the Passive and Active Rat Vagina Under Biaxial Loading, Annals of Biomedical Engineering 47 (2018) 272-281.
[21] E. Peña, P. Martins, T. Mascarenhas, R.M. Natal Jorge, A. Ferreira, M. Doblaré, B. Calvo, Mechanical characterization of the softening behavior of human vaginal tissue, Journal of the Mechanical Behavior of Biomedical Materials 4(3) (2011) 275-283.
[22] G.L. Clark, A.P. Pokutta-Paskaleva, D.J. Lawrence, S.H. Lindsey, L. Desrosiers, L.R. Knoepp, C.L. Bayer, R.L. Gleason, K.S. Miller, Smooth muscle regional contribution to vaginal wall function, Interface focus 9(4) (2019) 20190025.
[23] A.W. Caulk, J.D. Humphrey, S.-I. Murtada, Fundamental Roles of Axial Stretch in Isometric and Isobaric Evaluations of Vascular Contractility, Journal of biomechanical engineering 141(3) (2019) 0310081-03100810.
[24] S. White, J. Kiley, B. Visniauskas, S. Lindsey, K. Miller, **Biaxial Murine Vaginal Remodeling with Reproductive Aging**, Journal of Biomechanical Engineering (2022 (in press)).
[25] L. De Landsheere, C. Munaut, B. Nusgens, C. Maillard, C. Rubod, M. Nisolle, M. Cosson, J.-M. Foidart, Histology of the vaginal wall in women with pelvic organ prolapse: a literature review, International Urogynecology Journal 24(12) (2013) 2011-2020.
[26] M. Brieu, P. Chantereau, J. Gillibert, L. de Landsheere, P. Lecomte, M. Cosson, A nonlinear-elastic constitutive model for soft connective tissue based on a histologic description: Application to female pelvic soft tissue, Journal of the Mechanical Behavior of Biomedical Materials 58 (2016) 65-74.
[27] H.B. Henninger, C.J. Underwood, S.J. Romney, G.L. Davis, J.A. Weiss, Effect of elastin digestion on the quasi-static tensile response of medial collateral ligament, Journal of orthopaedic research 31(8) (2013) 1226-1233.

[28] S. Imayama, K. Nakamura, M. Takeuchi, Y. Hori, Y. Takema, Y. Sakaino, G. Imokawa, Ultraviolet-B irradiation deforms the configuration of elastic fibers during the induction of actinic elastosis in rats, Journal of dermatological science 7(1) (1994) 32-38.
[29] G. Imokawa, Y. Takema, Y. Yorimoto, K. Tsukahara, M. Kawai, S. Imayama, Degree of Ultraviolet-Induced Tortuosity of Elastic Fibers in Rat Skin Is Age Dependent, Journal of investigative dermatology 105(2) (1995) 254-258.
[30] A. Akintunde, K. Robison, D. Capone, L. Desrosiers, L. Knoepp, K. Miller, Effects of Elastase Digestion on the Murine Vaginal Wall Biaxial Mechanical Response, American Society of Mechanical Engineers 141(2) (2018).
[31] N.N. Kim, K. Min, M.A. Pessina, R. Munarriz, I. Goldstein, T.A. M, Effects of Ovariectomy and Steroid Hormones on Vaginal Smooth Muscle Contractility, International Journal of Impotence Research 16 (2004) 43-50.
[32] A. Huntington, K. Donaldson, R. De Vita, Contractile Properties of Vaginal Tissue, Journal of biomechanical engineering (2020).
[33] J.O. Marx, A.K. Brice, R.C. Boston, A.L. Smith, Incidence Rates of Spontaneous Disease in Laboratory Mice Used at a Large Biomedical Research Institution, Journal of the American Association for Laboratory Animal Science 52(6) (2013) 782-791.
[34] S. Abramowitch, A. Feola, Z. Jallah, P. Moalli, Tissue mechanics, animal models, and pelvic organ prolapse: a review, European Journal of Obstetric and Gynecological Reproductive Biology 144 (2009) 146-158.
[35] J.G. Fox, The Mouse in biomedical research, 2nd [upd. and rev.] ed., Academic Press, Amsterdam ;, 2007.
[36] R. Chia, F. Achilli, M. Festing, E. Fisher, The origins and uses of mouse outbred stocks, Nature Genetics 37 (2005) 1181-1186.
[37] S. Byers, Mouse Estrous Cycle Identification Tool and Images, PLoS ONE 7(4) (2012).
[38] K. Robison, C. Conway, L. Desrosiers, L. Knoepp, K. Miller, Biaxial Mechanical Assessment of the Murine Vaginal Wall Using Extension-Inflation Testing, Journal of Biomechanical Engineering 139(10) (2017).
[39] R. Gleason, S.P. Gray, E. Wilson, J. Humphrey, A Multiaxial Computer-Controlled Organ Culture and Biomechanical Device for Mouse Carotid Arteries, Journal of Biomechanical Engineering 126(6) (2005) 787-795.
[40] J. Ferruzzi, M. Bersi, J. Humphrey, Biomechanical phenotyping of Central Arteries in Health and Disease: Advantages of and Methods for Murine Models, Annals of Biomedical Engineering 41(7) (2013) 1311-1330.
[41] M. Amin, V. Le, J. Wagenseil, Mechanical Testing of Mouse Carotid Arteries: from Newborn to Adult, Journal of Visual Experiments (60) (2012).
[42] J. Ferruzzi, M.R. Bersi, J.D. Humphrey, Biomechanical Phenotyping of Central Arteries in Health and Disease: Advantages of and Methods for Murine Models, Annals of biomedical engineering 41(7) (2013) 1311-1330.
[43] M. Sherratt, Tissue elasticity and the ageing elastic fibre, The Official Journal of the American Aging Association 31(4) (2009) 305-325.
[44] E. Pack, J. Dubik, W. Snyder, A. Simon, S. Clark, R. De Vita, Biaxial Stress Relaxation of Vaginal Tissue in Pubertal Gilts, Journal of biomechanical engineering 142(3) (2019).
[45] C.K. Conway, H.J. Qureshi, V.L. Morris, E.K. Danso, L. Desrosiers, L.R. Knoepp, C.J. Goergen, K.S. Miller, Biaxial biomechanical properties of the nonpregnant murine cervix and uterus, Journal of Biomechanics 94 (2019).
[46] J. Humphrey, Cardiovascular Solid Mechanics: Cells, Tissues, and Organs, Springer, New York, 2002.
[47] S.E. White, Biaxial Basal Tone and Passive Testing of the Murine Reproductive System Using a Pressure Myograph, Jove-Journal of Visualized Experiments (150) (2019).
[48] A.J. DeMarsilis, T.A. Walji, J.A. Maedeker, K.V. Stoka, B.A. Kozel, R.P. Mecham, J.E. Wagenseil, C.S. Craft, Elastin Insufficiency Predisposes Mice to Impaired Glucose Metabolism, Journal of molecular and genetic medicine 8(3) (2014).
[49] T.D. Schmittgen, K.J. Livak, Analyzing real-time PCR data by the comparative CT method, Nature protocols 3(6) (2008) 1101-1108.
[50] A.J. Huntington, B. Udayasuryan, P. Du, S.S. Verbridge, S.D. Abramowitch, R.D. Vita, Smooth Muscle Organization and Nerves in the Rat Vagina: A First Look Using Tissue Clearing and Immunolabeling, Annals of biomedical engineering 50(4) (2022) 440-451.
[51] M. Weemhoff, K.L. Shek, H.P. Dietz, Effects of age on levator function and morphometry of the levator hiatus in women with pelvic floor disorders, International Urogynecology Journal 21(9) (2010) 1137-1142.
[52] D.E.E. Rizk, M.A. Fahim, Ageing of the female pelvic floor: towards treatment a la carte of the “geripause”, International Urogynecology Journal 19(4) (2008) 455-458.
[53] L. Lei, Y. Song, R. Chen, Biomechanical properties of prolapsed vaginal tissue in pre- and postmenopausal women, International Urogynecology Journal 18(6) (2007) 603-607.
[54] W. Badiou, G. Granier, P.-J. Bousquet, X. Monrozies, P. Mares, R. Tayrac, Comparative histological analysis of anterior vaginal wall in women with pelvic organ prolapse or control subjects. A pilot study, Including Pelvic Floor Dysfunction 19(5) (2008) 723-729.
[55] P. Takacs, M. Gualtieri, M. Nassiri, K. Candiotti, C. Medina, Vaginal smooth muscle cell apoptosis is increased in women with pelvic organ prolapse, Including Pelvic Floor Dysfunction 19(11) (2008) 1559-1564.
[56] S. Poncet, S. Meyer, C. Richard, J.-D. Aubert, L. Juillerat-Jeanneret, The expression and function of the endothelin system in contractile properties of vaginal myofibroblasts of women with uterovaginal prolapse, American journal of obstetrics and gynecology 192(2) (2005) 426-432.
[57] A.B.S. Clobes, J.O.L.M.D. DeLancey, D.M.M.D. Morgan, Urethral circular smooth muscle in young and old women, American journal of obstetrics and gynecology 198(5) (2008) 587.e1-587.e5.
[58] J.M. Perez, D.A. Rathz, N.N. Petrashevskaya, H.S. Hahn, L.E. Wagoner, A. Schwartz, G.W. Dorn, S.B. Liggett, β1-adrenergic receptor polymorphisms confer differential function and predisposition to heart failure, Nature medicine 9(10) (2003) 1300-1305.

[59] K.N. Bitar, S.B. Patil, Aging and gastrointestinal smooth muscle, Mechanisms of ageing and development 125(12) (2004) 907-910.
[60] J.W. Seawright, H. Sreenivasappa, H.C. Gibbs, S. Padgham, S.Y. Shin, C. Chaponnier, A.T. Yeh, J.P. Trzeciakowski, C.R. Woodman, A. Trache, Vascular Smooth Muscle Contractile Function Declines With Age in Skeletal Muscle Feed Arteries, Frontiers in physiology 9 (2018) 856-856.
[61] J. Xu, M. Sun, Y. Tan, H. Wang, H. Wang, P. Li, Z. Xu, Y. Xia, L. Li, Y. Li, Effect of matrix stiffness on the proliferation and differentiation of umbilical cord mesenchymal stem cells, Differentiation (London) 96 (2017) 30-39.
[62] N. Coll-Bonfill, U. Mahajan, E.V. Shashkova, C.-J. Lin, R.P. Mecham, S. Gonzalo, Progerin induces a phenotypic switch in vascular smooth muscle cells and triggers replication stress and an aging-associated secretory signature, GeroScience 45(2) (2023) 965-982.
[63] A. Orlandi, M.-L. Bochaton-Piallat, G. Gabbiani, L.G. Spagnoli, Aging, smooth muscle cells and vascular pathobiology: Implications for atherosclerosis, Atherosclerosis 188(2) (2006) 221-230.
[64] W. Fhayli, Q. Boëté, O. Harki, A. Briançon-Marjollet, M.-P. Jacob, G. Faury, Rise and fall of elastic fibers from development to aging. Consequences on arterial structure-function and therapeutical perspectives, Matrix biology 84 (2019) 41-56.
[65] O. Fritze, B. Romero, M. Schleicher, M.P. Jacob, D.-Y. Oh, B. Starcher, K. Schenke-Layland, J. Bujan, U.A. Stock, Age-Related Changes in the Elastic Tissue of the Human Aorta, Journal of vascular research 49(1) (2012) 77-86.
[66] M.A. Cattell, J.C. Anderson, P.S. Hasleton, Age-related changes in amounts and concentrations of collagen and elastin in normotensive human thoracic aorta, Clinica chimica acta 245(1) (1996) 73-84.
[67] S.D. Shapiro, S.K. Endicott, M.A. Province, J.A. Pierce, E.J. Campbell, Marked longevity of human lung parenchymal elastic fibers deduced from prevalence of D-aspartate and nuclear weapons-related radiocarbon, The Journal of clinical investigation 87(5) (1991) 1828-1834.
[68] M.P. Bendeck, F.W. Keeley, B.L. Langille, Perinatal accumulation of arterial wall constituents: relation to hemodynamic changes at birth, American journal of physiology. Heart and circulatory physiology 267(6) (1994) H2268-H2279.
[69] R. Rynkevic, P. Martins, L. Hympanova, H. Almeida, A.A. Fernandes, J. Deprest, Biomechanical and morphological properties of the multiparous ovine vagina and effect of subsequent pregnancy, (2017).
[70] C.K. Wieslander, S.I. Marinis, P.G. Drewes, P.W. Keller, J.F. Acevedo, R.A. Word, Regulation of Elastolytic Proteases in the Mouse Vagina During Pregnancy, Parturition, and Puerperium, Biology of reproduction 78(3) (2008) 521-528.
[71] P.G. Drewes, H. Yanagisawa, B. Starcher, I. Hornstra, K. Csiszar, S.I. Marinis, P. Keller, R.A. Word, Pelvic Organ Prolapse in Fibulin-5 Knockout Mice: Pregnancy-Induced Changes in Elastic Fiber Homeostasis in Mouse Vagina, The American journal of pathology 170(2) (2007) 578-589.
[72] K.T. Downing, M. Billah, E. Raparia, A. Shah, M.C. Silverstein, A. Ahmad, G.S. Boutis, The role of mode of delivery on elastic fiber architecture and vaginal vault elasticity: A rodent model study, Journal of the mechanical behavior of biomedical materials 29 (2014) 190-198.
[73] B. Dhital, K.T. Downing, F. Gul-E-Noor, Y. Landau, P. Rathod, S. Hirsch, E.J. Chang, G.S. Boutis, Alterations of elastin in female reproductive tissues arising from advancing parity, Archives of Biochemistry and Biophysics 666 (2019) 127-137.
[74] B. Kelly, P. Chowienczyk, Vascular Compliance, Second ed.2004.
[75] S. Sugita, T. Matsumoto, Multiphoton microscopy observations of 3D elastin and collagen fiber microstructure changes during pressurization in aortic media, Biomechanics and modeling in mechanobiology 16(3) (2017) 763-773.
[76] W. Badiou, G. Granier, P.-J. Bousquet, X. Monrozies, P. Mares, R. de Tayrac, Comparative histological analysis of anterior vaginal wall in women with pelvic organ prolapse or control subjects. A pilot study, International Urogynecology Journal 19(5) (2008) 723-729.
[77] J.A. Karam, D.V. Vazquez, V.K. Lin, P.E. Zimmern, Elastin expression and elastic fibre width in the anterior vaginal wall of postmenopausal women with and without prolapse, BJU international 100(2) (2007) 346-350.
[78] M.K. Boreham, C.Y. Wai, R.T. Miller, J.I. Schaffer, R.A. Word, Morphometric analysis of smooth muscle in the anterior vaginal wall of women with pelvic organ prolapse, American Journal of Obstetrics and Gynecology 187(1) (2002) 56-63.
[79] A. Huntington, S.D. Abramowitch, P.A. Moalli, R. De Vita, Strains induced in the vagina by smooth muscle contractions, Acta biomaterialia 129 (2021) 178-187.
[80] M. McCarthy, A.P. Raval, The peri-menopause in a woman's life: a systemic inflammatory phase that enables later neurodegenerative disease, Journal of neuroinflammation 17(1) (2020) 1-317.
[81] H.L. Brooks, D.P. Pollow, P.B. Hoyer, The VCD mouse model of menopause and perimenopause for the study of sex differences in cardiovascular disease and the metabolic syndrome, Physiology (Bethesda, Md.) 31(4) (2016) 250-257.
[82] R. Patel, J.D. Moffatt, E. Mourmoura, L. Demaison, P.T. Seed, L. Poston, R.M. Tribe, Effect of reproductive ageing on pregnant mouse uterus and cervix: Effect of reproductive ageing on pregnant uterus and cervix, The Journal of physiology 595(6) (2017) 2065-2084.
[83] C.M. Markey, C.L. Michaelson, E.C. Veson, C. Sonnenschein, A.M. Soto, The mouse uterotrophic assay: A reevaluation of its validity in assessing the estrogenicity of bisphenol A, Environmental health perspectives 109(1) (2001) 55-60.
[84] B. Kozel, H. Wachi, E. Davis, R. Mecham, Domains in tropoelastin that mediate elastin deposition in vitro and in vivo, J Biol Chem 278(20) (2003)18491-8
[85] J. Schindelin, I. Arganda-Carreras, E. Frise, V. Kaynig, M. Longair, T. Pietzsch, S. Preibisch, C. Ruden, S. Saalfeld, B. Schmid, J. Tinevez, D. White, V. Hartenstein, K. Eliceiri, P. Tomancak, A. Cardona, Fiji: an-open source platform for biological-image analysis, Nat Methods, 9(7) (2012) 676-82

[86]. J. Bredfeldt, Y. Liu, C. Pehlke, M. Conklin, J. Szulczewski, D. Inman, P. Keely, R. Nowak, T. Mackie, K. Elceiri, Computation segmentation of collagen fibers from second-harmonic generation images of breast cancer, J Biomed Opt, 19(1), (2014)
[87] Y. Liu, A. Keikhosravi, G. Mehta, C. Drifka, K. Eliceiri, Methods for quantifying fibrillar collagen alignment, Methods Mol Biol, (2017), 429-451